# SIMPLE MODELS FOR CHARACTERIZATION OF MECHANICAL PROPERTIES BY NANOINDENTATION

## Jaroslav Menčík

.

**Chapter 4**

# SIMPLE MODELS FOR CHARACTERIZATION OF MECHANICAL PROPERTIES BY NANOINDENTATION

### *Jaroslav Menčík*
University of Pardubice, Czech Republic

## ABSTRACT

Nanoindentation provides information about mechanical properties from indenter load and displacement, measured during loading and unloading. This chapter brings an overview of important models and formulae used in the evaluation of these measurements. The main topics are: approximation of load-depth curves, determination of contact stiffness, depth and area, hardness and elastic modulus, obtaining of yield strength and stress-strain curves from indentation data, information from the work of indentation, models for the response of coated or surface-treated components, models for the response of viscoelastic materials and procedures for obtaining their parameters from tests under monotonic and harmonic load, as well as for the determination of viscosity in creep tests.

## 1. INTRODUCTION

Nanoindentation, or – generally – instrumented indentation or depth-sensing indentation, provides information about mechanical properties of tested specimens from indenter load $F$ and displacement $h$ measured during loading and unloading. All quantities, such as contact depth and area, hardness, elastic modulus, yield strength or parameters of viscoelastic response, are calculated from the $F$-$h$ data or $F$-$h$-$t$ history using suitable models. Thus, the quality of these models is very important for the quality and accuracy of results. A well-known example is the improvement in the determination of contact stiffness by applying a power-law to the unloading curve, as proposed by Oliver and Pharr (1992), instead of the previously used linear fit.

This chapter gives an overview of important models used in depth-sensing indentation. Besides the basic formulae, also less known approaches and characteristic quantities are

presented. The main topics are: approximation of load-depth curves, determination of contact stiffness, depth and area, hardness and elastic modulus, work of indentation, yield strength and stress-strain curves, models for the response of coated or surface-treated components, and models for viscoelastic materials. The response of these materials, whose testing by nanoindentation becomes more and more popular, is discussed here for monotonic as well as harmonic load. The chapter ends with models for creep and the determination of viscosity.

At first, some general comments must be made. The models should not be more complex than necessary – with respect to the purpose of measurement. If one needs to determine certain material constant, e.g. elastic modulus, which will serve as a standard, the model should be as accurate as possible. Often, however, the main aim of measurement is just to compare various materials or conditions of surface treatment, or to assess the influence of an external factor, such as temperature or magnetic field. In such cases, simpler models may be used. The choice of suitable characteristics can reduce the number of variables, which must be known with high accuracy. Very useful are normalized or non-dimensional quantities. They are more general than "absolute" ones and make possible comparison of tests done under different conditions. For example, the energy, spent in indentation, corresponds to a particular load. However, the indentation energy per unit volume of imprint is the same for all indents created by the same type of pointed indenter in the same homogeneous material. Another example: indentation response of a coated specimen depends on the properties of the coating and substrate, but also on the depth of penetration. If, however, this depth is related to the coating thickness, it is posible to combine the results obtained with coatings of various thicknesses.

The use of dimensionless quantities has one more advantage. According to the theory of similarity, the number of non-dimensional quantities for expressing a physical law is usually smaller than the number of dimensional quantities. This can make the empirical formulae simpler and reduce the necessary number of experiments, or even allow the combination of results from different kinds of tests. More about dimensional analysis and similarity can be found in books, e.g. Barenblatt (1996) or Szirtes (1997), or in a paper and a comprehensive review by Cheng and Cheng (1999, 2004), devoted especially to indentation measurements. Also in this chapter non-dimensional quantites will be used wherever suitable.

In the following sections, models and formulae used in the evaluation of nanoindentation measurements will be given. As for the principles of depth-sensing indentation, the reader is referred to the literature, e.g. Doerner and Nix (1986), Oliver and Pharr (1992 and 2004), or a monograph by Fischer-Cripps (2002). Also the international standard ISO 14577 can be mentioned here. Other works will be quoted in the individual sections. As the number of papers, published on the topic is vast, the author apologizes for using only some of them, the main reason being the effort to keep this overview brief.

## 2. LOAD-DISPLACEMENT CURVES

Loading curve for indentation into homogeneous elastic-plastic specimens (Figure 1) can be expressed as

$$F = k_1 h^m ; \tag{1}$$

$F$ is indenter load, $h$ is indenter displacement (depth of penetration), and $k_l$, $m$ are constants. For homogeneous elastic materials and a cylindrical punch, $m = 1$. For spherical indenters and small penetrations, $m = 1.5$ (also for paraboloids), while for pointed indenters (Vickers or Berkovich (3-sided) pyramid or a cone), $m = 2$. As the real „pointed" indenters have usually small blunting at the tip, the measured displacement $h$ is sometimes replaced by the effective depth of penetration,

$$h_{eff} = h + \xi \, ; \tag{2}$$

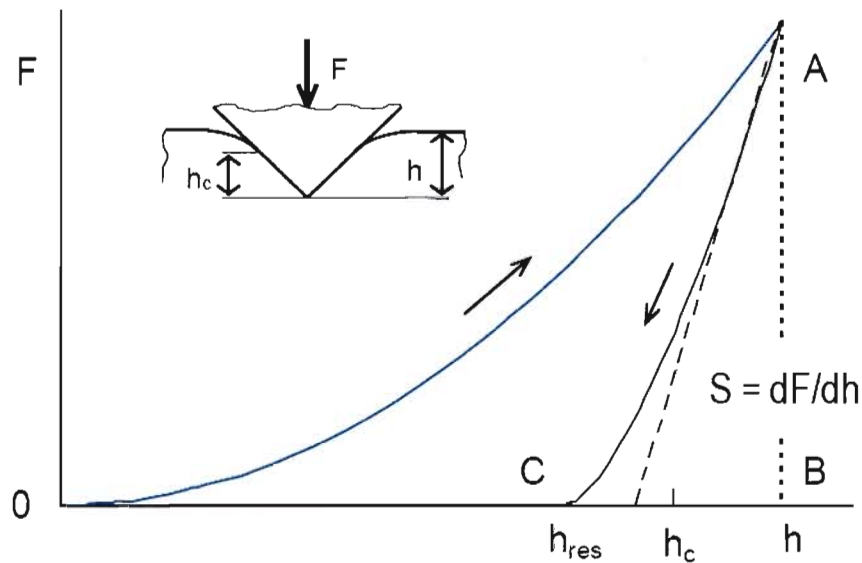with the correction term $\xi$ obtained by fitting the $F(h)$ curve.



Figure 1. Loading and unloading curves of an indentation test – a schematic.

The approximation (1) is suitable for elastic-plastic deformations. (Its relationship to the elastic modulus and hardness is shown in Section 5.) However, in materials with strain hardening, in specimens with treated surface (or even with a thin oxidic layer on the surface), or for indenters whose shape deviates from the ideal one, the exponent $m$ can differ from the above values, and must be found by fitting the measured data. For inhomogeneous specimens or with time-dependent response, or if discontinuous processes occur (e.g. cracking), the loading curve can have a more complicated shape.

Unloading curve is usually approximated as

$$F = k_u (h - h_{res})^n \, ; \tag{3}$$

$k_u$, $n$ and the residual depth $h_{res}$ of the imprint after unloading are constants, obtained by regression fitting the unloading data. The unloading is mostly elastic, and the curve (3) holds also for reloading, which is elastic. Thus, the curve (3) should correspond to the curve (1) for elastic loading, with $h$ replaced by $(h - h_{res})$; the exponents in both formulae should be identical, $m = n$. While this is true for spherical indenter or cylindrical punch under low loads, significant differences appear for pointed indenters (e.g. Berkovich), with $n$ ranging usually between 1.2 and 1.6 (instead of 2.0). As shown by Pharr and Bolshakov (2002) and Oliver

and Pharr (2004), the reason are plastic deformations induced in the specimen during loading. As a consequence, the unloaded imprint is not exactly pyramidal, but somewhat convex. During reloading, such surface comes into contact with the indenter gradually, similarly to the contact of a spherical indenter with a plane, and thus with lower exponent $n$.

The actual unloading curve sometimes deviates from the approximation (3), especially at its low-load part. A role can be played by adhesion and friction between the indenter and specimen, by creep, after-effects or irreversible processes during unloading, or by stress-induced phase transformations, leading to jumps in the $F(h)$ curve. For the same reasons, the calculated residual depth $h_{res}$ can differ from the actual value.

Curves (1) and (3) are expressed in the coordinate system force – displacement. It is also possible to plot them in nondimensional coordinates, using normalized quantities

$$F_{norm} = F/F_{max} \,, \ h_{norm} = h/h_{max} \,, \ \text{or} \ h_{norm} = (h - h_{res})/(h_{max} - h_{res}) \,, \tag{4}$$

varying between 0 and 1. The shape of $F_{norm}$–$h_{norm}$ curves is similar to $F$– $h$. It is also possible to express nondimensional depth as $(h - h_{res})/h_{max}$. Normalized quantities enable the comparison of response for various loads or materials.

## 3. CONTACT STIFFNESS

Two kinds of contact stiffness are used in depth-sensing indentation tests: unloading and harmonic.

Unloading contact stiffness $S$ is defined as

$$S \ = \ \frac{dF}{dh} \,, \tag{5}$$

and it is determined for the maximum load (Figure 1) by fitting the upper part of the monotonic unloading curve by Eq.(3) and making the derivative. Unloading contact stiffness is necessary for the determination of contact depth and elastic modulus. The determination of $S$ in elastic-plastic materials is straightforward. With respect to Eq. (3), it can be expressed from the parameters of unloading curve as

$$S = n \, F \, / \, (h - h_{res}) \,. \tag{6}$$

In viscoelastic materials, a correction for delayed deforming must usually be made (cf. Section 9).

Harmonic contact stiffness $S_f$ can be measured by nanoindentation devices, which superimpose a small harmonic signal (amplitude several nm or a fraction of a millinewton) on the monotonically increasing basic load (so-called Continuous Stiffness Measurement mode, CSM, or Dynamic Mechanical Analysis, DMA). Basically, $S_f$ is defined as the ratio of the load and depth amplitudes of the small oscillations,

$$S_f = \frac{F_0}{h_0} \; ; \tag{7}$$

subscript $f$ denotes the excitation frequency. However, in viscoelastic materials a lag appears between the harmonic stress and strain, and this can also be considered in the data processing (see Section 10).

In the CSM (or DMA) mode, $S_f$ can be measured during the whole loading process (Figure 2). Harmonic contact stiffness is suitable for studying the depth distribution of properties and for materials, whose response depends on time, for example polymers.

In elastic-plastic materials, $S_f$ has the same value as the unloading stiffness $S$, while in viscoelastic materials both quantities can differ, depending on the material and excitation frequency.
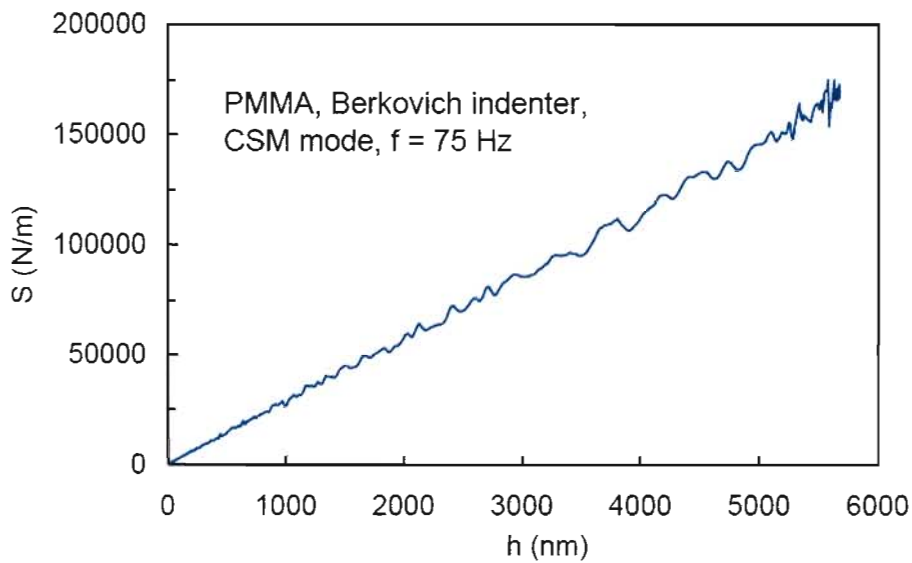


Figure 2. Harmonic contact stiffness S as a function of indenter penetration h into PMMA (after Menčík et al., 2005).

With respect to Eq. (1), the depth course of contact stiffness $dF/dh$ in homogeneous specimens can be approximated by a simple function of type

$$S(h) = m \, k_l \, h^{m-1} \; . \tag{8}$$

For example, the contact stiffness for a pointed indenter ($m = 2$) is directly proportional to depth.

This can be utilized in processing the data obtained in the CSM (or DMA) mode. The course of measured harmonic contact stiffness is usually undulated (Figure 2), and so also are all quantities calculated from it, e.g. harmonic elastic modulus. Fitting $S_f(h)$ by Eq. (8) makes it smooth, which gives a smoother course of the derived quantities.

## 4. CONTACT DEPTH AND AREA

In depth-sensing indentation into elastic-plastic materials, the contact depth $h_c$ (Figure 1) is determined from the total depth $h$ according to the general formula

$$h_c = c_1 h - c_2 \frac{F}{S} , \qquad (9)$$

where $F$ is the maximum load, and $S$ is the contact stiffness at the beginning of unloading.

In the mostly used approach, proposed by Oliver and Pharr (1992), $c_1 = 1$ and $c_2 = 0.75$. According to some authors, these constants work well for stiffer materials, but give underestimated values for soft materials with substantial plastic flow and pile-up effects. For them, the following values were recommended (Bec et al., 1996, Fujisawa and Swain, 2006): $c_1 = 1.2$ and $c_2 = 1$. The contact depth can be normalized as $h_{norm} = h_c/h$.

The contact area $A$ is calculated from the contact depth $h_c$ as

$$A = f(h_c) . \qquad (10)$$

For an ideal pointed indenter (Figure 3a),

$$A = \pi a^2 = k\, h_c^{\,2} , \qquad (11)$$

where $a$ is the contact radius of the equivalent cone, related to the contact depth as $a = h_c \tan \alpha$; $\alpha$ is the semiapical tip angle. For Vickers or Berkovich indenter, $\alpha = 70.3°$ and $k = 24.5$. For spherical indenters (Figure 3b) and small depths of penetration,

$$A = \pi a^2 = \pi (2rh_c - h_c^2) ; \qquad (12)$$

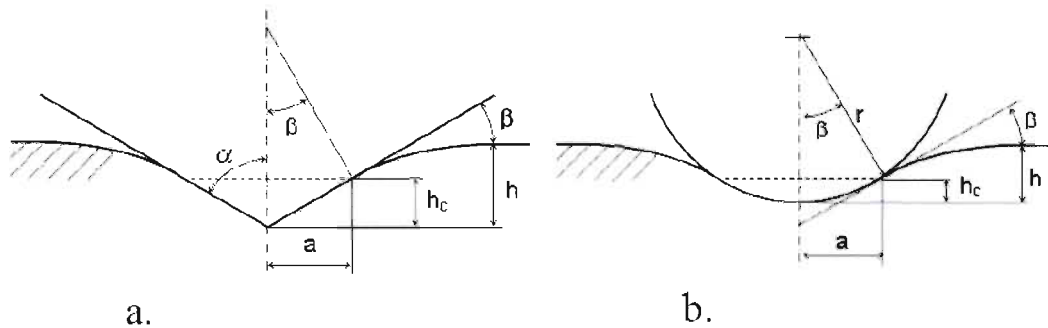$r$ is the tip radius. For small contact depths, $A \approx 2\pi r h_c$.



Figure 3. Contact geometry: a – pointed indenter, b – spherical indenter.

Often, the tip shape is not ideal, and indenters must be calibrated by tests on real materials. An often used approximation for pointed indenters is:

$$A(h_c) = k h_c^{\,2} + C_1 h_c^{\,1} + C_2 h_c^{\,1/2} + C_3 h_c^{\,1/4} + \dots \qquad (13)$$

## 5. HARDNESS AND ELASTIC MODULUS

In depth-sensing indentation tests, hardness is defined as the mean contact pressure under the loaded indenter,

$$H = p_m = \frac{F}{A} ; \tag{14}$$

$F$ is the load and $A$ is contact area. There are also other definitions of indentation hardness; more about basic concepts, relation of hardness to plastic and elastic properties, etc., can be found in the classic book by Tabor (1951) and papers by Sakai (1993, 1999). Small-size effects are treated in Wei and Hutchinson (2003).

Elastic modulus is determined from the formula

$$E_r = \frac{\sqrt{\pi}}{2\beta} \frac{S}{\sqrt{A}} ; \tag{15}$$

$\beta$ is the correction factor for the indenter shape; $\beta = 1$ for indenters with circular cross-section (cylindrical punch, sphere or a cone), and $\beta = 1.034$ for Berkovich indenter (Oliver and Pharr, 1992). Commonly, unloading stiffness (5) is used for $S$. However, if dynamic properties are studied using the CSM (DMA) mode, harmonic contact stiffness (7) is inserted into (15), giving so-called harmonic or complex modulus (for details, see Herbert et al. (2008) and Section 10). Formula (15) is based on Sneddon's analysis (1965) for penetration of various indenters into elastic half-space. $E_r$ means reduced (composite) modulus, from which the specimen modulus $E$ is calculated using the formula

$$\frac{1}{E_r} = \frac{1-v^2}{E} + \frac{1-v_i^2}{E_i} , \tag{16}$$

expressing that the total contact compliance consists of the compliance of the specimen (no subscript) and the indenter (subscript $i$); $v$ is Poisson's ratio.

Combination of Eqs. (14) and (15) yields a very simple check of material homogeneity. If $E$ and $H$ do not change with depth, then also the ratio $F(h)/S^2(h)$ must be constant.

Elastic and plastic properties are, together with the indenter shape, also decisive for the shape of loading curve. The penetration of a spherical indenter into elastic materials is described by Eq. (1) with $m = 3/2$ and the constant

$$k_l = (4/3) E_r r^{1/2} , \tag{17}$$

following from the theory for elastic contact of spheres; cf. Johnson (1985); $r$ is the radius of indenter tip, and $E_r$ is the reduced modulus defined by Eq. (16). If the deformations in a test are only elastic (i.e. if the loading and unloading curves overlap), Equation (1) with the constant $k_l$ from Eq. (17) can be used directly for obtaining the reduced modulus from the curve $F(h)$; otherwise Eq. (15) must be used. Pointed indenters usually cause also plastic

deformations, so that the loading curve (1) depends on the elastic modulus and hardness. Hainsworth et al. (1996) have proposed the following relationship:

$$k_l = E_r \left( \Phi \sqrt{E_r/H} + \Psi \sqrt{H/E_r} \right)^{-2} , \tag{18}$$

with constants $\Phi$ and $\Psi$. For Berkovich or Vickers indenter with the tip semiangle $\alpha = 70.3°$, Malzbender et al. (2000) have derived the values $\Phi = 0.202$ and $\Psi = 0.638$. Formula (18) follows from the relationship $F = k_l h^2$ with the total depth $h$ expressed as a sum of the contact depth $h_c$ and elastic displacement $h_s$ of the surface at the perimeter of the contact, $h = h_c + h_s$. According to Sneddon (1965), $h_s = \varepsilon F/S$, where $\varepsilon = 2(\pi - 2)/\pi = 0.72$ for a conical indenter. Contact depth is related to the load and hardness via Eq. (14) with $A = 24.5 \, h_c^2$. Combination of these formulae with (14) and (15) allow one to express the contact stiffness $S$, and then $h_c$, $h_s$, $h$ and $k_l$ as a function of $F$, $E_r$ and $H$. On this topic, see also Oliver (2001) and Pharr et al. (2009).

## 6. WORK OF INDENTATION

Useful information can be gained from energies involved in indentation processes. Mechanical work is proportional to the area below the load–displacement curve (Figure 1). The total work of indentation $W_{tot}$ (area under the curve 0ABC0) consists of the plastic (unrecoverable) energy $W_{pl}$ (area 0AC0) and elastic work $W_{el}$ released during unloading (area CABC):

$$W_{tot} = W_{pl} + W_{el} . \tag{19}$$

These energies can be obtained by numerical integration of the measured $F(h)$ values, or – approximately – by analytical integration of the loading and unloading curves (1) and (3):

$$W_{tot} = \int_0^h F(h) dh \approx \int_0^h k_l h^m dh = \frac{1}{m+1} F h , \tag{20}$$

$$W_{el} \approx \int_{h.res}^h k_u (h - h_{res})^n dh = \frac{1}{n+1} F (h - h_{res}) . \tag{21}$$

The plastic work is calculated as

$$W_{pl} = W_{tot} - W_{el} . \tag{22}$$

The $F(h)$ diagram can also be used to extract the energies related to special phenomena during the indentation, like formation of cracks, delamination of a coating, or load-induced phase transformations.

The knowledge of total work also makes possible the determination of constants in the loading curve (1) even without the regression fitting:

$$m = \frac{F\,h}{W_{tot}} - 1 \quad : \qquad k_l = \frac{F}{h^m} \; .$$

(23)

The unloading curve, however, depends also on the residual depth of penetration, $h_{res}$, and its constants must be obtained by regression fitting of the measured data. Here, one must keep in mind that the curves (1) and (3) are approximations only, which characterize the "average" course of $F(h)$ at the beginning of unloading, and later can deviate from the actual shape.

The energies $W_{tot}$, $W_{pl}$ and $W_{el}$ correspond to a particular test, with particular load and depth of penetration. More general information is obtained by normalizing them. For example, it is possible to define elasticity index $\omega_{el}$ and plasticity index $\omega_{pl}$ as the ratio of the returned (el) or dissipated (pl) energy to the total work of indentation:

$$\omega_{el} = \frac{W_{el}}{W_{tot}} \quad : \qquad \omega_{pl} = \frac{W_{pl}}{W_{tot}} = 1 - \omega_{el} \; .$$

(24)

The work of indentation can be related to the volume of residual impression,

$$w_1 = \frac{W_{tot}}{V_{res}} \; .$$

(25)

$V_{res}$ can be calculated from the residual depth and contact area (obtained from hardness as $A = F/H$). The simplest situation is for pointed indenters, where $V_{res} \approx Ah_{res}/3$. For them and for ideally plastic materials, $h_{res} = h$ and the work per unit indentation volume corresponds to hardness, $w_1 = H$.

The energies in indentation processes are also related to depths. Comparing the curves for loading (1) and unloading (3), Menčík and Swain (1994) have introduced the parameter

$$\vartheta = \frac{h_{res}}{h} = 1 - \frac{m+1}{n+1}\frac{W_{el}}{W_{tot}} \; ,$$

(26)

which can be used to characterize the permanent damage caused in various materials by indentation. Ni et al. (2004) used finite element modelling and derived the following relationship for indentation with a spherical indenter:

$$\vartheta = \frac{h_{res}}{h} = \frac{W_{tot} - W_{el}}{W_{tot}} \; .$$

(27)

Since the exponents $m$ and $n$ for the loading and unloading curves in spherical indentation are approximately the same, it is obvious that Eq. (27) is a special case of a more universal relationship (26).

As the load-unload curves are self-similar for a pointed indenter and homogeneous material, $\omega_{el}$, $\omega_{pl}$, $w_1$ and $a_1$ do not depend on the load and can be used as material characteristics, for example in theoretical study of indentation processes or for prediction of damage by impact. More ideas about energies in indentation processes, including their relationship to hardness, elastic modulus, plasticity and other properties, can be found, e.g., in Sakai (1993, 1999), Ni et al. (2004), Malzbender (2005), Tan (2006), and Chen and Bull (2009).

# 7. YIELD STRENGTH AND STRESS–STRAIN CURVES

An important material characteristic is hardness $H$. However, it is no basic material property. A more general quantity is the yield stress $Y$. Even better is the „$\sigma - \varepsilon$" diagram, saying how the yield stress develops with strain. Numerous authors have dealt with the determination of yield stress and stress-strain curves from indentation. Tabor (1951) and Johnson (1970) were among the first, followed by Menčik and Swain (1994), Yu and Blanchard (1996), Mesarovic and Fleck (1999), Herbert et al. (2001, 2006), Ogasawara et al. (2005), just to name some of them. Stress-strain curves of polymeric materials were treated, e.g., by Hochstetter et al. (2003). In addition to yield strength, some papers also present procedures for the determination of strain-hardening exponent, for example Field and Swain (1993), Kucharski and Mróz (2001), Ma et al. (2003), Cao and Lu (2004), and Gao (2006). However, new materials, such as shape-memory alloys, can exhibit even more complicated response. In this section, only a simple method for the construction of $\sigma - \varepsilon$ curves, based on Johnson's approach (1970, 1985), will be described (Menčik, 2006).

The stress field under any indenter is inhomogeneous, and must be characterized by some representative stress and strain, $\sigma_{rep}$ and $\varepsilon_{rep}$. The mean contact pressure $p_m$ is very suitable for $\sigma_{rep}$, while the expression for representative strain will depend also on the indenter shape.

The distribution of stresses under a pointed indenter (Figure 3a) is self-similar, and only one value of $p_m$ is obtained for a homogeneous material, regardless the indenter depth. The representative strain can be expressed as $\varepsilon_{rep} = k \tan\beta$, where $k$ is a constant and $\beta$ is the angle between the specimen surface and the indenter ($\beta = 90° - \alpha$, where $\alpha$ is the semiapical angle; see Figure 3a). Tabor (1951) has recommended $k = 0.2$, based on the comparison of indentation and tensile experiments. For Berkovich or Vickers indenters, $\beta = 19.7°$, so that the measured hardness and yield stress $Y$ pertain to a rather high characteristic strain, $\varepsilon_{rep} \approx 7\%$.

Under a spherical indenter (Figure 3b), the mean contact pressure and strains increase with the depth of indenter penetration, and can be used to construct the stress–strain curves. The representative strain is usually expressed as the ratio of contact radius $a$ and indenter radius $r$: $\varepsilon_{rep} = k(a/r)$, where $k$ is a constant (often, $k = 0.2$ is assumed). For small penetrations, the deformations are elastic. The maximum shear stress acts below the surface, and plastic deformations appear here if the mean contact pressure attains $p_m \approx 1.1Y$. As long as the plastically deformed zone is small and surrounded by elastically deformed material, the "load-displacement" curve is the same as in elastic state. With increasing load, the plastic

region grows and the *F–h* curve departs gradually from the elastic course. Since some instant, plastic deforming spreads up to the free surface around the indenter (fully developed plastic flow).

The stresses beneath indenter are tri-axial. If the stress-strain curve, based on indentation tests, should resemble the common $\sigma - \varepsilon$ diagram for uniaxial loading, it must be constructed in coordinates $\sigma_{eq} - \varepsilon_{rep}$. The equivalent stress $\sigma_{eq}$ can be calculated from $p_m$ as

$$\sigma_{eq} = p_m / \Phi(\varepsilon_{rep}, E, Y, \nu...) \quad ; \tag{28}$$

the function $\Phi$ depends on the degree of deforming ($\varepsilon_{rep}$), elastic modulus $E$, basic value of yield strength $Y$ and Poisson's ratio $\nu$. Equation (28) is generalization of the well-known relationship between hardness $H$ (= $p_m$) and uniaxial yield stress $Y$ in soft metals, $H = CY$, where the constraint factor $C$ expresses the fact that the mean contact pressure, needed to cause plastic flow, must be higher than the yield stress (Tabor, 1951).

The stress-strain curve (Figure 4) can be constructed from the data obtained by spherical indenter for a series of loads or using the continuous measurement of properties with depth. It consists of two asymptotes (for small and large strains) and an intermediate part.
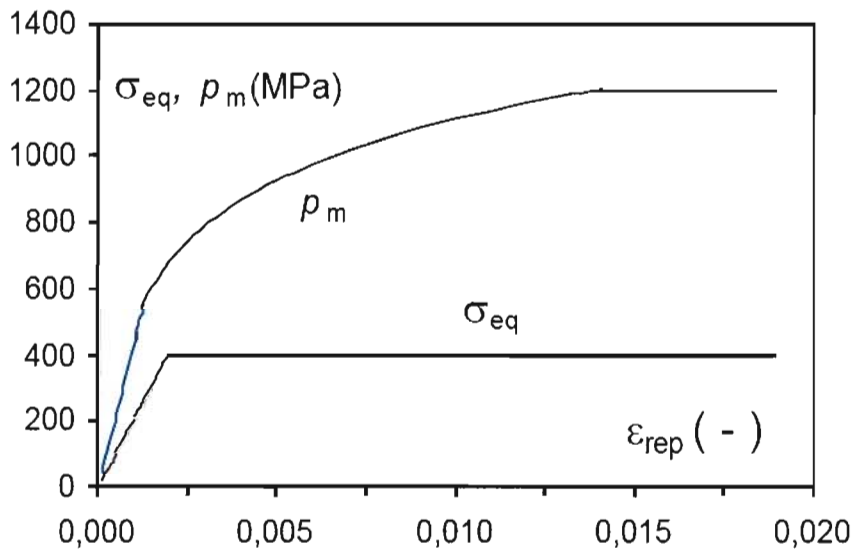


Figure 4. Equivalent stress $\sigma_{eq}$ and mean contact pressure $p_m$ as functions of representative strain $\varepsilon_{rep}$. Ideal elastic-plastic material without strain hardening. $E_r$ = 210 GPa. $Y$ = 400 MPa. spherical indenter. $r$ = 50 μm. (After Menčík, 2006.).

*Asymptote 1 – elastic deformations.* As long as the equivalent stress is lower than the yield strength, the relationship between the equivalent stress and representative strain is linear,

$$\sigma_{eq} = E \varepsilon_{rep} . \tag{29}$$

For elastic contact of a sphere with a plane, the Hertz formula can be used:

$$p_m = \frac{4}{3\pi} E_r \frac{a}{r} .$$                                                                (30)

Combination of Eqs. (28) – (30) gives the proportionality constant $\Phi$ for $\varepsilon_{rep} = 0.2a/r$:

$$\Phi = 20 / (3\pi) .$$                                                                                        (31)

Mesarovic and Fleck (1999) have revealed by extensive FEM modeling that, despite of the onset of plastic flow at $p_m = 1.1Y$, the relationship $p_m(\varepsilon_{rep})$ for spherical indentation is linear as long as $p_m < 1.6Y$.

*Asymptote 2 – soft materials, full plastic flow.* In soft materials ($E/H > 40$), the fully plastic flow is developed soon. In this case, the constraint factor is a constant, $\Phi \approx 3$, and the yield stress is calculated as

$$Y(\varepsilon_{rep}) = \sigma_{eq}(\varepsilon_{rep}) \approx p_m(\varepsilon_{rep})/3 .$$                    (32)

Note. Some authors use the value $\Phi = 2.9$, the difference being about 3%.

*Intermediate part – elastic-plastic deformations.* For hard materials ($E/H < 40$), or for small representative strain $\varepsilon_{rep}$ compared to the elastic strain capacity $\varepsilon_Y = Y/E$ of the material, the plastically deformed zone is small and surrounded by a relatively large elastic region. The elastic strains are not negligible compared to plastic ones. The constraint factor $\Phi$ depends on the ratio of the representative strain (imposed by the indenter) to the material strain capacity, $\varepsilon_{rep}/\varepsilon_Y$. The simplest expression for $\Phi$ is based on the model of an infinite elastic–plastic body with a spherical cavity under internal pressure, as developed by Johnson (1970); see also his monograph (1985) or Fischer-Cripps (2002):

$$\Phi = A + B \ln(C \varepsilon_{rep} / \varepsilon_Y) ,$$                                                        (33)

where $A$, $B$ and $C$ are constants. If $\varepsilon_Y$ is not known in advance, it is easier to determine the yield stress $Y(\varepsilon_{rep})$ directly from the expression (Menčík and Swain, 1994, Menčík, 2006)

$$\frac{p_m(\varepsilon_{rep})}{Y(\varepsilon_{rep})} = A + B \ln\left( C \frac{E}{Y_0} \varepsilon_{rep} \right) ,$$      (34)

with the constants: $A \approx 4/3$, $B \approx 2/3$, and $C \approx 5/3$ for $\varepsilon_{rep} = 0.2a/r$ (or 0.2 $\tan\beta$ for Berkovich indenter). Equation (34) must be solved for $Y$ numerically (for given $p_m$, $\varepsilon_{rep}$ and $E$); this can be done using solver, present in various software. The procedure could be improved, for example by considering the influence of Poisson's ratio, as given in the original Johnson's model of the expanding cavity (1970), or by implementing the extended model by Gao (2006), which respects strain hardening, indenter shape and the size of the imprint.

When constructing the stress-strain curve, it is reasonable first to plot $\sigma_{eq}$ in wider ranges of $\varepsilon_{rep}$ using approximations (30) – (34), and then to find their appropriate limits. The constant $\Phi$ for elastic deformations (= $20/3\pi$) should be used for $p_m \leq 1.6Y$. An example of curves

$p_m(\varepsilon_{rep})$ and $\sigma_{eq}(\varepsilon_{rep})$, obtained for given material data, is depicted in Figure 4. Vice versa, it is also possible to obtain material parameters from the empirical $p_m(\varepsilon_{rep})$ curve (Menčík, 2006).

Approximation of the curve $\sigma_{eq}(\varepsilon_{rep})$ or its part by the expression

$$Y(\varepsilon) \;=\; Y_0\,(\varepsilon/\varepsilon_0)^x \qquad\qquad (35)$$

enables the determination of strain-hardening index $x$ for elastic-plastic materials.

From other recent works on this topic, Ogasawara et al. (2005), Basu et al. (2006), and Wang and Rokhlin (2006) can be mentioned.

## 8. MODELS FOR THE RESPONSE OF COATED OR SURFACE-TREATED COMPONENTS

Nanoindentation is very suitable for the determination of mechanical properties of coatings or treated surfaces. However, the response during indentation is influenced by the properties of both the coating and substrate. The measured $E$ or $H$ values change from the values corresponding to the coating or surface alone (for negligible depth of penetration), to the substrate value for the penetration depths much larger than the thickness of the coating or film (Figure 5).
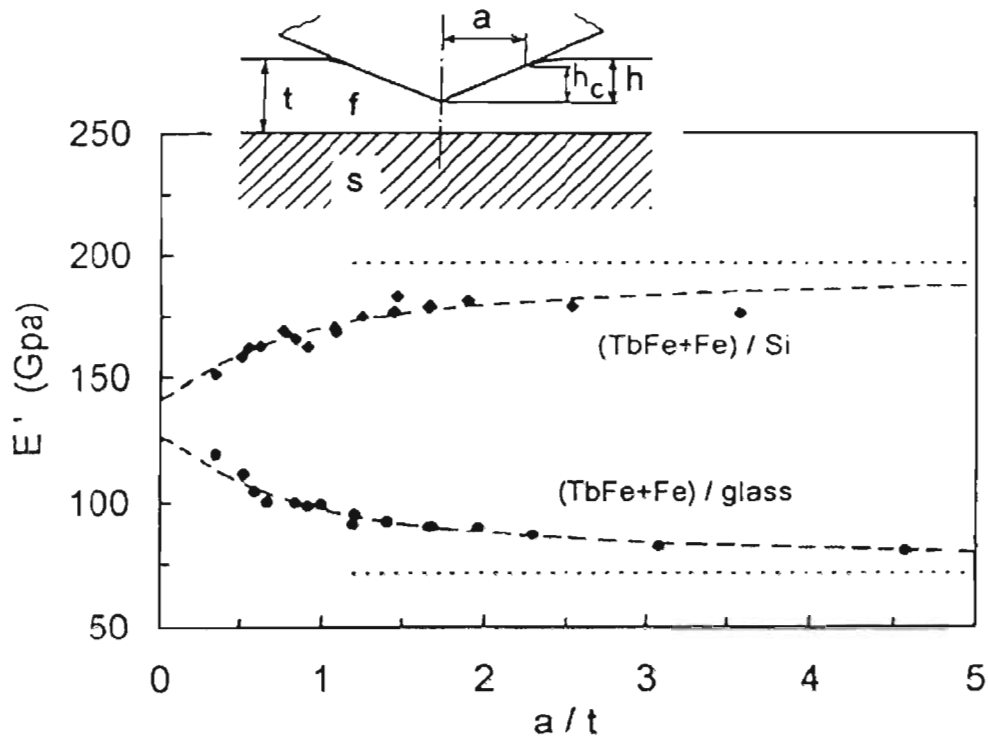


Figure 5. Apparent elastic modulus E' as a function of indenter penetration into a coating (TbFe+Fe) on a stiffer substrate (Si) and on a more compliant substrate (glass). a – contact radius, s – substrate, f – film (coating) of thickness t. (Adapted from Menčík et al., 1997).

Thus, the penetration should be much smaller than the coating thickness, especially when the coating is harder or stiffer than the substrate. Often it is recommended that the depth of penetration should not exceed 1/10 of the film thickness, for the substrate influence to be negligible. This is a difficult task, particularly for thin films. Moreover, the apparent elastic modulus is influenced from the beginning of indentation. Therefore, the response is usually measured for various depths, and the genuine coating property is obtained by extrapolating the measured values to zero depth. The devices working in the CSM (DMA) mode are especially useful, as they can yield the necessary series of $E(h)$ or $H(h)$ values in one test. The coating or film properties are best determined with pointed indenters, where the impression shape does not depend on the depth of penetration.

The apparent value of property "$X$" (hardness, elastic modulus, etc.), measured for the indenter penetration into depth $\xi$, can generally be expressed as

$$X(\xi) = X_f\, w_f(\xi) + X_s\, w_s(\xi) , \tag{36}$$

where $X_f$ and $X_s$ are the values corresponding to the film (or surface) and substrate, and $w_f(\xi)$ and $w_s(\xi)$ are non-dimensional weight factors, characterizing the influence of the coating and substrate on the indenter response at depth $\xi$. This depth can be measured in length units; however, it is better to use the relative depth, expressed as $\xi = h/t$ or $a/t$, where $h$, $t$ and $a$ are the depth of penetration, film thickness and contact radius.

Another, only formally different, expression is

$$X(\xi) = X_f\Phi(\xi) + X_s\big[1 - \Phi(\xi)\big] , \tag{37}$$

where

$$\Phi(\xi) = \frac{X(\xi) - X_s}{X_f - X_s} \tag{38}$$

is a dimensionless weight function, which decreases from 1 for $\xi = 0$ (or $h = 0$) to zero for $\xi \to \infty$ (or $h \gg t$). Thus, knowing the substrate property $X_s$ from independent measurements, one can obtain the coating property $X_f$ as a regression constant by fitting the $X(\xi)$ values for various depths by the expression (37) with a suitable function $\Phi$.

Several weight functions have been proposed. For elastic modulus, Doerner and Nix (1986) used a simple exponential function,

$$\Phi(\xi) = 1 - \exp\big[-(b\xi)\big] , \tag{39}$$

where $\xi = t/h$, and $b$ is a constant obtained by fitting the measured $E(\xi)$ values. The authors used compliances $1/E_f$ and $1/E_s$ for $X_f$ and $X_s$ in Eq. (37) – according to the idea of coating and substrate acting as two springs in series.

Menčik et al. (1997) tested several functions for the modulus, and recommended the expression based on the theoretical analysis of a layered elastic medium by Gao et al. (1992):

$$\Phi_G = \frac{2}{\pi}\arctan \xi + \frac{1}{2\pi(1-\nu)}\left[(1-2\nu)\xi\ln\frac{1+\xi^2}{\xi^2} - \frac{\xi}{1+\xi^2}\right] ;$$

(40)

$\xi = t/a$ and $\nu$ is Poisson's ratio; $X$ in Eqs. (37) and (38) corresponds to elastic modulus. The suitability of this function is demonstrated in Figure 6. Some other expressions can be found in Menčík (1996] and Menčík et al. (1997). As illustrated in the previous Figure 5, the accuracy in the determination of film modulus can be increased by making the tests for the film deposited on a stiffer substrate and on a more compliant one; the genuine modulus will lie between both empirical $E_f$ values.
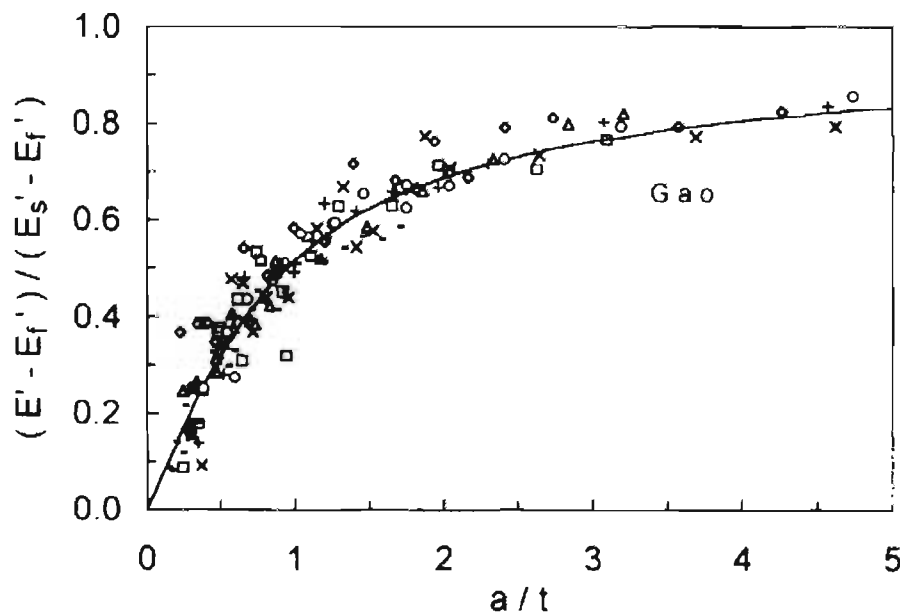


Figure 6. Gao's function (40) plotted together with the measured values of apparent elastic modulus for 14 various combinations „material + substrate": a – radius of contact, t – film thickness; subscripts f and s denote the film and substrate, respectively. (After Menčík et al., 1997).

When determining coating hardness, two cases with basically different response can be distinguished: soft coating on a hard substrate, and a hard coating on a ductile substrate. While the plastic deformations are limited to the coating in the former case, a hard coating on a soft substrate deforms elastically and plunges into a relatively larger volume of plastically deformed substrate, and, eventually, breaks. There are many papers about the topic. The simplest empirical approximations were proposed by Bhattacharya and Nix (1988):

$$U_j(x,y) = \frac{1}{d}\int_{-x}^{\infty} V[(\rho_j^2 + z^2)^{1/2}]dz$$

(41)

for hard films on softer substrates, and

$$\rho_j = [(x-x_j)^2 + (y-y_j)^2]^{1/2}$$

(42)

for soft films on hard substrates; $c_1$ and $c_2$ are constants, $\xi = h/t$, and $X_f$, $X_s$ are $H_f$ and $H_s$. Korsunsky et al. (1998) proposed the following weight function:

$$\Phi(\xi) \;=\; \frac{1}{1 + k\xi^2} \;,$$ 

(43)

where $\xi = h/t$ and $k$ is a fitting parameter.

Two other approximations are based on physical models. Jönsson and Hogmark (1984) proposed the weight functions in Eq. (36) using the "area-law of mixtures":

$$w_f = A_f /A \;,\; w_s = A_s /A \;,$$ 

(44)

where $A$ is the projected area of contact, $A_f$ is its part where the indenter load is carried by the film, and $A_s$ is the contact area around $A_f$, where the load is carried by substrate; $A_f + A_s = A$. This model was developed originally for a brittle film on a ductile substrate, with easy distinguishable $A_f$ and $A_s$.

Burnett and Rickerby (1987) proposed the weight functions for hardness as the ratio of influenced volumes in the coating and substrate:

$$w_f = V_f /V \;,\; w_s = V_s /V \;;$$ 

(45)

$V_f$ and $V_s$ is the volume of plastically deformed material in the film and substrate; $V = V_f + V_s$ is the total deformed volume. This approach is more suitable for ductile films on hard substrates. Several methods have been proposed for the determination of $V_f$ and $V_s$ from the indentation dimensions, film thicknesses and mechanical properties of the coating and substrate.

Further information and references on the determination of mechanical properies of coatings and layered systems can be found in papers by Malzbender and de With (2000), Rar et al. (2001), Saha and Nix (2002), Bec et al. (2006), Huber et al. (2006), Page and Bull (2006), Wei et al. (2009), and Sakai (2009).

# 9. VISCOELASTIC-PLASTIC MATERIALS – RESPONSE TO MONOTONIC LOAD

Deformations of many materials depend not only on the load magnitude, but also on its duration and time course. Such materials are called viscoelastic or viscoelastic-plastic. Their properties may be obtained by nanoindentation, but proper quantities must be used for the characterization, and the arrangement of tests must respect the time-dependence of response.

For example, the indenter continues penetrating into the specimen even under constant load (Figure 7), so that hardness (14) is no more a constant, but decreases with the time under load, $H = H(t)$. After unloading, recovery (or backcreep) often occurs. Moreover, due to delayed response, the unloading part of the $F–h$ curve is often distorted – more convex than for elastic materials (dotted curve in Figure 8).
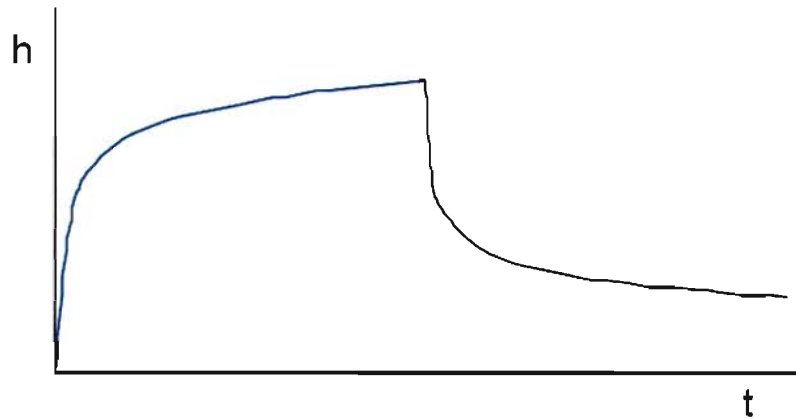
Figure 7. Characteristic response of viscoelastic-plastic materials to load (a schematic). h – depth of penetration (generally, displacement). t – time. Left part depicts delayed deforming and creep under constant load, right part depicts the course of deformations after unloading.
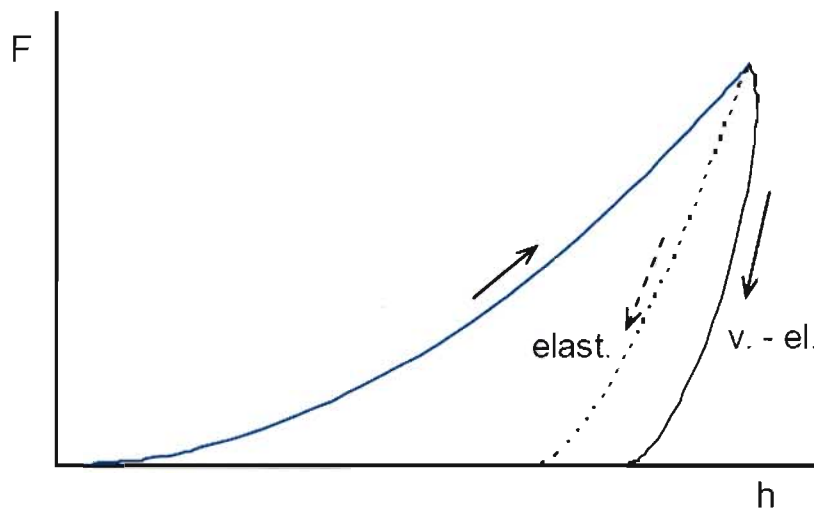


Figure 8. Typical loading and unloading indentation curves for elastic (elast.) and viscoelastic (v.-el.) material: a schematic. F – load, h – indenter penetration.

As a consequence, the apparent contact stiffness $S$, determined from the slope of unloading curve, is higher than the actual value. This can lead to errors in the determination of contact depth and area and all quantities depending on them.

The influence of viscoelastic after-effects can be reduced in various ways. Often, a dwell is inserted between the loading and unloading. According to Chudoba and Richter (2001), the effect of delayed deformation on the unloading curve may be neglected if the creep velocity has decreased so that the depth of penetration grows less than 1% per minute. The influence of creep at the end of dwell can also be mitigated by using the effective contact stiffness $S$, as proposed by Feng and Ngan (2002):

$$\frac{1}{S} = \frac{1}{S_{app}} + \frac{\dot{h}_d}{\left|\dot{F}_u\right|} ; \tag{46}$$

$S_{app}$ is the apparent stiffness, obtained from the unloading curve by the standard procedure described in Section 3 ($S_{app}$ is denoted $S$ there); $\dot{h}_d$ is the indenter velocity at the end of dwell, and $\dot{F}_u$ is the load decrease rate at the beginning of unloading.
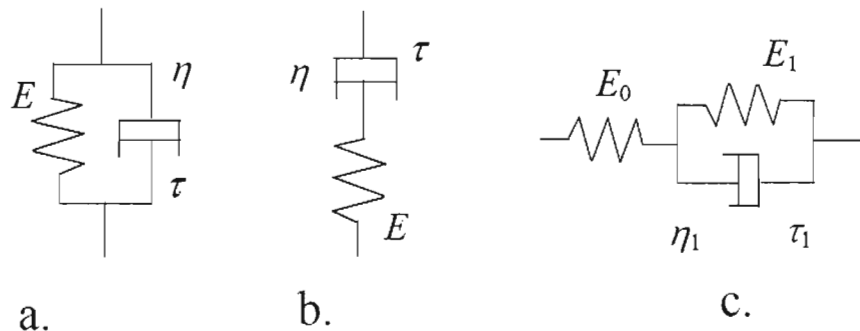


Figure 9. Rheological models: a – Kelvin-Voigt body. b – Maxwell body. c – Standard Linear Solid. E – elastic modulus, η – viscosity, τ – relaxation (or retardation) time.

A disadvantage of this approach is that the indenter depth at the beginning of unloading (after the dwell) is larger than at the end of loading. This results in larger contact area and lower apparent hardness. Therefore, it is recommended to use relatively fast loading followed immediately by fast unloading (Cheng and Cheng, 2005). Nevertheless, it is generally insufficient to characterize materials, which flow under load, only by a single value of hardness or elastic modulus. Also a special characteristic, the strain-rate sensitivity index $m$ (Goble and Wolff, 1993), based on the relationship $\sigma \propto \sigma_s{}^m$, as observed for the steady-state creep in some materials, has only limited use. Better are standard rheological models, created from springs and dashpots (Figure 9), which are universal and can also be used in commercial software for the finite element analysis.

## 9.1. Models for Linear Viscoelastic Response

The basic elements are a spring and a dashpot. In a spring, the strain is directly proportional to stress, while in a dashpot, proportionality exists between the stress and strain rate. A simple combination is the Kelvin-Voigt body (Figure 9a), suitable for modelling of delayed deforming by decreasing rate. The Maxwell body (Figure 9b) can characterize the processes of stress relaxation. For modelling of real bodies, more complex models are often necessary, for example Standard Linear Solid (Figure 9c). The pertinent equations can be found in monographs, such as Findley et al. (1976), Tschoegl (1989) or Haddad (1995). Therefore, only the expressions relevant to indentation testing will be given here.

The formulae for viscoelastic response to indentation can be derived using the analogy between elastic and viscous deforming (cf. Section 11). This approach was first applied by Radok (1957) and Lee and Radok (1960), who utilised the elastic solutions of contact problems, but replaced the elastic constants by a viscoelastic integral operator; see also Johnson (1985).

The relationship between the non-decreasing indenter load and the depth of penetration into viscoelastic material can be expressed generally as

$$h^{\mathrm{m}}(t) = K \, \psi (F, J, t) , \qquad (47)$$

where $m$ and $K$ are constants characterizing the indenter geometry. For a flat cylindrical punch of diameter $2r$, $m = 1$ and $K_{\mathrm{P}} = 1/(2r)$. For a spherical indenter, $m = 3/2$ and $K_{\mathrm{S}} = 3/(4\sqrt{r})$, where $r$ is the indenter tip radius. For pointed indenters (conical, Berkovich or Vickers), $m = 2$ and $K_{\mathrm{C}} = \pi/(2 \tan \alpha)$; $\alpha$ is the semiangle of indenter tip or of equivalent cone. $\psi (F, J, t)$ is a response function depending on the load magnitude and history and on so-called creep compliance function $J(t)$ for the pertinent material model (see later). For constant load $F$ acting after step change from 0, the response function $\psi$ simply equals the product of load and creep compliance function,

$$\psi (t) = F \, J(t), \qquad (48)$$

so that

$$h^{\mathrm{m}}(t) = K \, F \, J(t) . \qquad (49)$$

If the load varies (monotonically), the response function $\psi (F, J, t)$ for linearly viscoelastic materials is obtained as

$$\psi (t) = \int_{0}^{t} J(t - u)[dF/du]du \; ; \qquad (50)$$

$u$ is a dummy variable for integration.

The simplest model for reversible delayed deforming consists of a spring in series with a Kelvin-Voigt body. The creep compliance function for this standard linear solid (SLS, Figure 9c), is

$$J(t) = C_0 + C_1 [1 - \exp(- t / \tau_1)] . \qquad (51)$$

$C_0$ and $C_1$ are compliance constants; $C_0$ corresponds to the instantaneous component of deformation and $C_1$ to the delayed deformation; $\tau_1$ is the time constant of the system (retardation time), related to the compliance $C_1$ of the spring and dynamic viscosity $\eta_1$ of the dashpot in the Kelvin-Voigt body as $\tau_1 = \eta_1 C_1$. At the instant of loading, $J(0) = C_0$, while for very long time, $J(t \to \infty) = C_0 + C_1$.

More complicated reversible response can be modelled by adding more Kelvin-Voigt bodies (Figure 10):

$$J(t) = C_0 + \sum C_j [1 - \exp(- t / \tau_j)] \; ; \; \tau_j = \eta_j C_j , \, j = 1, 2 \ldots n . \qquad (52)$$

Often also irreversible deformations appear, which can be: 1) time-independent plastic deformations, caused by high stresses under concentrated load, or: 2) time-dependent creep, known, for example, in asphalt or glasses and metals at relatively high temperatures. The time-independent plastic deforming is characterized by a slider in Figure 10.
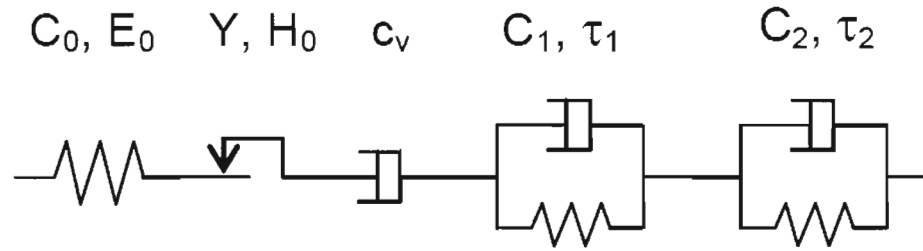
$$C_0, E_0 \quad Y, H_0 \quad c_v \quad C_1, \tau_1 \quad\quad C_2, \tau_2$$

Figure 10. General Standard Linear Solid. C – compliance, E – elastic modulus, Y – yield strength, H – hardness, $c_v$ – viscous compliance, $\tau$ – retardation time.

Its characteristic (yield strenth $Y$ or hardness $H$) is contained together with the characteristic for instantaneous elastic response $(E)$ in the compliance constant $C_0$. Combination of Eq. (18) and (1) with Eq. (49), written for a pointed indenter and the instantaneous part of deformation (i.e. $J(t) = C_0$), gives the following approximate relationship between $C_0$ and elastic-plastic parameters (Menčík et al., 2009):

$$C_0 = \frac{2\tan\alpha}{\pi}\frac{1}{E_r}\left(\Phi\sqrt{E_r/H} + \Psi\sqrt{H/E_r}\right)^2 . \tag{53}$$

Time-dependent irreversible viscous deformation can be characterized by a dashpot of viscosity $\eta$, arranged in series with the other bodies (Figure 10). The creep compliance function for the dashpot alone is

$$J(t) = c_v t , \tag{54}$$

where $c_v$ is the viscous compliance. If this dashpot is connected in series with the general standard linear solid (52), the creep compliance function is

$$J(t) = C_0 + c_v t + \Sigma C_j [1 - \exp(-t/\tau_j)]\} . \tag{55}$$

Formula (55) is universal. Specific response can be described by leaving only some elements in the model. The first two terms alone $(C_0 + c_v t)$ correspond to the Maxwell body (Figure 9b). In a special case the model (55) contains only the spring $C_0$ and characterizes instantaneous (time-independent) deformations. For fully reversible elastic deformations, the compliance $C_0$ can be expressed by means of elastic modulus:

$$C_0 = \frac{1-\nu^2}{E} ; \tag{56}$$

the term $(1 - \nu^2)$ accounts for the triaxial state of stress around the indenter; the relationship for uniaxial stress would be $C_0 = 1/E$. Equation (56) is valid for a rigid indenter. If the indenter cannot be considered stiff compared to the specimen, the expression $E/(1 - \nu^2)$ must be replaced by reduced modulus $E_r$ defined by Eq. (16). Analogously to Eq. (56), also the compliances of other Kelvin-Voigt bodies could be expressed as reciprocals of moduli, $C_j = 1/E_j$.

The viscous compliance $c_v$ in Eqs. (54), (55) is related to dynamic viscosity $\eta$ as

$$c_v = (1 - v)/(2\eta) , \tag{57}$$

as it follows from the condition of compatibility of Eq. (57) with (49) and (56) and from the fact that $\eta$ expresses the proportionality between shear stress and strain rate.

The load response of viscoelastic materials is often modelled by the finite element method. In elastic-plastic analysis, Young modulus $E$ and Poisson's ratio $v$ are mostly used. Some FEM programs also work with the shear modulus $G$ and bulk modulus $K$, which are related to the elastic modulus and Poisson's ratio as follows:

$$G = E/[2(1 + v)] , K = E/[3(1 - 2v)] . \tag{58}$$

The finite element method enables analysis of viscoelastic materials and parts as well. Commercial computer codes, such as Ansys, Marc or Abaqus, use Prony series, defined as

$$y(t) = \Sigma B_j \exp(- t/\tau_j) ; \tag{59}$$

$B_j$ and $\tau_j$ are constants. The creep compliance function (52) can then be written as

$$J(t) = B_\infty + \Sigma B_j \exp(- t/\tau_j) , \text{ where } B_\infty = C_0 + \Sigma C_j , \text{ and } B_j = - C_j . \tag{60}$$

Compliances of Kelvin-Voigt bodies can be given in nondimensional form, as well:

$$J(t) = B_\infty [1 + \Sigma D_j \exp(- t/\tau_j)] , \text{ with } D_j = B_j/B_\infty . \tag{61}$$

If the software for viscoelastic analysis uses shear modulus $G$ and bulk modulus $K$, these quantities may also be expressed in a form of series:

$$G(t) = G_\infty + \Sigma G_j \exp(- t/\tau_{G,j}) , K(t) = K_\infty + \Sigma K_j \exp(- t/\tau_{K,j}) . \tag{62}$$

Generally, $G$ and $K$ can have different time course and different number of terms in the series. Often, various simplifying assumptions are used; e.g. incompressibility ($v = 0,5$) or constant Poisson's ratio ($v =$ const), and only the time dependence of $G$ or $E$ is assumed.

## 9.2. Determination of Model Parameters

The constants in spring-and-dashpot models must be determined by experiment, for example by fitting the time course of indenter penetration $h^m(t)$ by Eq. (47) with a suitable creep compliance function $J(t)$. Various procedures have been proposed during the last twenty years. Among the first authors, Lucas et al. (1997), Strojny et al. (1998) and other given in Moody et al. (1998) can be named. Formulae for flat punch indentation were proposed by L. Cheng et al. (1998, 2000) and Strojny and Gerberich (1998), while pointed indenters were dealt by Shimizu et al. (1999), Cheng and Cheng (1999, 2005a), Zhang et al. (2005) and Oyen

and Cook (2003). Methods for spherical indenters were developed by L. Cheng et al. (1998) and Oyen (2005, 2006). L. Cheng et al. (2005) brings closed-form formulae for relaxation testing and creep testing by spherical indenters. Formulae for all three indenter shapes are given in Sakai and Shimizu (2001), while Cheng and Cheng (2005b) have derived solution for axisymmetric indenters of arbitrary profile. Huber and Tyulyukovskiy (2004) and Tyulyukovskiy and Huber (2006) developed a procedure for identification of viscoplastic properties, using neural networks. Further papers can be found in the proceedings edited by Baker et al. (2001) and Wahl et al. (2005), and some will be mentioned later in this section.

The methods for determination of viscoelastic parameters under monotonic loading can be divided into two basic groups: with constant load and constant load rate. Here only the case with constant load will be described, which is based on the theory from the previous section and leads to simple, but universal formulae, applicable for various indenter shapes.

For constant load after a step change, Eq. (49) can be used directly. Unfortunately, the load increase from 0 to the nominal value always lasts some time, and this influences the following response under constant load, more at the beginning (Lee and Knauss, 2000). However, if the load grows by constant rate and the duration of load increase is short compared to the retardation time, Equation (49) may be used also, just with slightly modified creep compliance function, as it will be shown further.

For ramp loading with constant load rate, $dF/dt = R = const$, Equation (50) gives

$$\psi(t) = R\int_0^t J(t-u)du \cdot \tag{63}$$

The response under constant load following the ramp loading is then

$$\psi(t) = R\int_0^{t_R} J(t-u)du , \tag{64}$$

where $t_R$ (= $F/R$) is the duration of load increase. Equation (64), valid for $t \geq t_R$, was obtained by superposition of two integrals (63) for loads growing by constant rate $R$: the first load starts at $t = 0$, while the other, acting in the opposite direction, starts at time $t_R$. Thus, for $t > t_R$, the load is constant, $F(t \geq t_R) = Rt - R(t - t_R) = Rt_R$. The application of Eq. (64) on the general standard linear solid (55) gives for $t \geq t_R$:

$$\psi(t) = F\{ C_0 + \Sigma C_j [1 - \rho_j \exp(- t/\tau_j)]\} = F J'(t) , \tag{65}$$

where $\rho_j$ is so-called ramp correction factor, as introduced by Oyen (2005, 2006):

$$\rho_j = ( \tau_j /t_R) [\exp(t_R /\tau_j) - 1] . \tag{66}$$

The modified creep compliance function $J'(t)$ in Eq. (65) differs from Eq. (52) only by the factors $\rho_j$ at exponential terms. For fast loading, with short load increase compared to the retardation times ($t_R \ll \tau_j$), the ramp correction factor $\rho_j$ is close to 1; it attains 1.025 for $t_R/\tau_j = 0.05$ and 1.05 for $t_R/\tau_j = 0.1$, and grows rapidly for higher ratios $t_R/\tau_j$.

The response function for the universal model (55) is (Menčík et al.. 2009):

$$\psi(t) = F\{C_0 + c_v(t - t_R/2) + \Sigma C_j[1 - \rho_j \exp(-t/\tau_j)]\} = F J''(t) ; \qquad (67)$$

the term $-t_R/2$ expresses the fact that the viscous component of the penetration at the end of the load-increase period ($t = t_R$) corresponds only to the average force growing from 0 to $F$.

The response function (65) or (67) is then inserted into Eq. (47). The constants can be obtained by minimizing the sum of the squared differences between the measured and calculated $h^m(t)$ values. However, the actual procedure must be modified. In Eq. (67), several terms appear, which do not depend on time: $C_0$, $c_v t_R/2$ and $C_j$. Regression analysis cannot determine them individually, but only as a whole; otherwise incorrect values could be obtained. Moreover, the terms $C_j \rho_j$ also occur here, with the still unknown ramp correction factors $\rho_j$. From a curve-fitting point of view, Equation (65), divided by $F$, corresponds to the Prony series (60) with $B_j = - C_j \rho_j$ and $B_\infty = C_0 + \Sigma C_j$. After obtaining the constants $B_0$, $B_j$ and $\tau_j$ from the measured data, the constants $\rho_j$, $C_0$ and $C_j$ can be calculated. The number of elements in the model can be verified from the duration of backcreep after unloading. The procedure is described in Menčík et al. (2009), and the quality of fit is illustrated in Figure 11.

If a new material is investigated, it is reasonable to fit the experimental $h(t)$ data by various creep compliance functions and choose the model with the best fit. The optimum parameters in each model can be found using a special program or a solver present in universal software such as Excel or Matlab. For models with only a few constants ($n \leq 4$), solver easily finds the "best" parameters ($C_0$, $C_1$, $\tau_1$...). With more constants, various „optimum" values of parameters are sometimes found depending on their starting values used in the search.
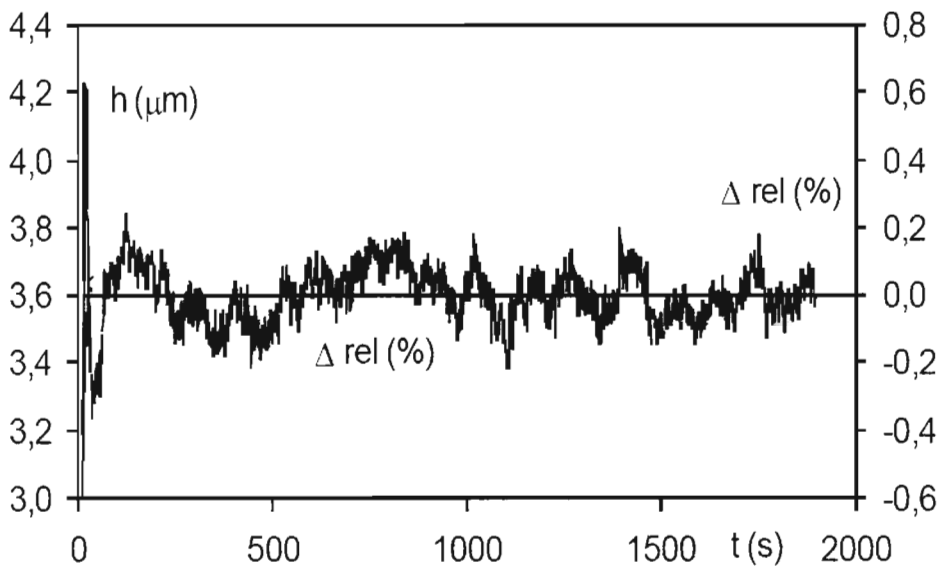


Figure 11. Penetration of Berkovich indenter into PMMA under constant load: measurement and approximation (spring + 3 Kelvin-Voigt bodies in series). Both curves (of „logarithmic" character) overlap: the relative differences [$\Delta_{rel} = (h_{measured} - h_{calculated})/h_{measured}$] do not exceed several tenths of a percent.

The differences between $J(t)$ curves for individual fits are often negligible. It is thus possible to choose fix retardation times $\tau_j$, scaled in decades; for example $\tau_1 = 1$ s, $\tau_2 = 10$ s, $\tau_3 = 100$ s, etc. Solver then must seek only the constants $C_0$, $C_1$, etc. In such case, one should remember that they are no true physical constants, but parameters in the model, valid only for some range of loading time. Generally, the test for obtaining a model should last as long as the time-dependent processes or as the duration of load action in the assumed application. Thermal stability of the measuring device is sometimes the limiting factor.

If several models give acceptable results, the "optimum" model can be chosen with respect to its future use. Generally, it should not be more complicated than necessary. Useful is the knowledge of typical properties of Kelvin-Voigt bodies. Every K-V body, with the response described by expression $C_j[1 - \exp(-t/\tau_j)]$, is active within about two orders of time; roughly for $0.03 < t/\tau_j < 3.0$. For example, $1 - \exp(-0.03) \approx 0.03$. Therefore, for $t/\tau_j < 0.03$, the body hardly started reacting, and till this time it behaves as if it were stiff. On the other hand, $1 - \exp(-3) \approx 0.95$, so that for $t/\tau_j > 3$ nearly the full deformation is reached, and the resultant response ($h$) correponds to the spring of compliance $C_j$ alone.

Slightly different approaches to the determination of parameters in rheological models by indentation can be found, e.g., in Giannakopoulos (2006), Lu et al. (2003), Zhang et al. (2005), and Dub and Trunov (2008).


# 10. VISCOELASTIC MATERIALS – RESPONSE TO HARMONIC LOAD

Typical of viscoelastic materials exposed to harmonic (sinusoidal) load is the shift between stress and strain (Figure 12) and dissipation of energy. Both phenomena depend on the material and also on frequency. The pertinent characteristics can be obtained by indentation devices, which use small additional harmonic load (CSM or DMA mode). In this section, basic definitions will be presented, as well as formulae for principal rheological models.

The response of viscoelastic materials to harmonic load is usually described by two quantities: phase angle and modulus. The phase angle $\delta$ (Figure 10) expresses the shift between stress and strain.
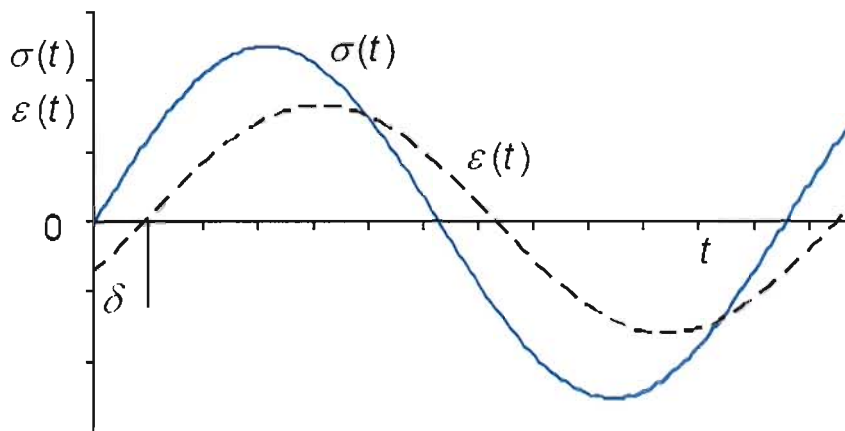


Figure 12. Response of a viscoelastic material to harmonic loading (a schematic). $\sigma(t)$ – stress. $\varepsilon(t)$ – strain. t – time. $\delta$ – shift between $\sigma$ and $\varepsilon$.

The modulus, which characterizes the material stiffness, consists of two components: storage modulus $E'$, which is in phase with the strain, and the loss modulus $E''$, which is 90° out of phase with strain; see, e.g., Haddad (1995) or Herbert et al. (2008):

$$\sigma_0 = (E' + i\,E'')\,\varepsilon_0 = E^* \varepsilon_0 \,, \ \tan\delta = E'' / E' ; \qquad (68)$$

$\sigma_0$ and $\varepsilon_0$ is the stress and strain amplitude, and $i$ is imaginary unit; $\tan\delta$, called loss factor, is a measure of damping in linear viscoelastic materials. Storage modulus, together with loss modulus, form complex dynamic modulus of amplitude

$$E^* = \sqrt{E'^2 + E''^2} = \sigma_0/\varepsilon_0 \ ; E' = E^* \cos\delta,\, E'' = E^* \sin\delta. \qquad (69)$$

In the $\sigma - \varepsilon$ coordinate system, one loading cycle is depicted by an ellipse. The energy, stored in a volume unit of material during a half cycle is

$$U_s = \tfrac{1}{2} E' \varepsilon_0^2 \,, \qquad (70)$$

and the energy dissipated in a volume unit during a complete cycle, is

$$U_d = \pi E'' \varepsilon_0^2 \,. \qquad (71)$$

The phase angle $\delta$ and complex modulus $E^*$ depend on the excitation frequency. The response of a material can be described by a rheological model, whose parameters are obtained by fitting the values of $E^*(\omega)$ and $\tan\delta(\omega)$, measured at various frequencies; $\omega = 2\pi f$ is angular frequency and $f$ is frequency. The formulae expressing $\tan\delta$ and $E^*$ as functions of frequency depend on the model and will be shown here for several important cases (Haddad, 1995), (Menčík et al., 2004).

## 10.1. Principal Models

*Kelvin-Voigt body (K-V, Figure 9a)*
The strain $\varepsilon$ is the same in the spring and the dashpot. The total stress $\sigma$ equals the sum of the stress in the spring (in phase with the strain) and the stress in the dashpot (preceding the strain by 90°), so that it precedes the strain by some phase angle $\delta$. The body is also characterized by complex modulus $E^*$ or compliance $C^*$ (= $1/E^*$).

$$\tan\delta = \omega\tau \,, \ E^* = E'\sqrt{1 + \tan^2\delta} = E'\sqrt{1 + (\omega\tau)^2} \qquad ; \qquad (72\text{a,b})$$

$\tau$ is the retardation time, calculated as $\tau = \eta/G$.

*Maxwell body (M, Figure 9b)*

The stress $\sigma$ is the same in the spring and dashpot. The total strain $\varepsilon$ is the sum of the strain in the spring (in phase with the stress) and in the dashpot (lagging behind the stress by 90°). The resultant strain is delayed by the angle $\delta$. The other characteristic is the complex modulus $E^*$ or compliance $C^*$ (= $1/E^*$):

$$\tan \delta = 1/\omega\tau\,, \quad E^* = E'\Big/\sqrt{1 + \tan^2 \delta} = E'\Big/\sqrt{1 + (\omega\tau)^2}\,. \tag{73a,b}$$

*Standard Linear Solid (SLS, Figure 13)*

The same stress $\sigma(t)$ acts in both the spring and Kelvin-Voigt body. The total strain $\varepsilon(t)$ equals the vector sum of the strain in the spring „0" (in phase with the stress) and the strain of the K-V body, which lags behind the stress by the angle $\delta_1$, given by Eq. (72). The resultant phase angle (Figure 13b) and complex modulus can be obtained from the formulae (Menčík et al., 2004):

$$\tan \delta = \left( \frac{1}{E_1} \frac{\omega\tau_1}{1 + (\omega\tau_1)^2} \right) \Big/ \left( \frac{1}{E_0} + \frac{1}{E_1} \frac{1}{1 + (\omega\tau_1)^2} \right)\,, \tag{74a}$$

$$\frac{1}{E^*} = \sqrt{ \left( \frac{1}{E_0} + \frac{1}{E_1} \frac{1}{1 + (\omega\tau_1)^2} \right)^2 + \left( \frac{1}{E_1} \frac{\omega\tau_1}{1 + (\omega\tau_1)^2} \right)^2 }\,. \tag{74b}$$

The terms $E_0$ and $E_1$ correspond to stiffnesses of individual springs. Similarly to Section 9, they may be replaced by compliances, defined as $C^* = 1/E^*$, $C_0 = 1/E_0$, and $C_1 = 1/E_1$.

As it follows from Eqs. (74), single standard linear solid can describe the changes in response only in a limited range of frequencies. For relatively slow processes, with $(\omega\tau)^2 \ll 1$, the resistance of the dashpot is negligible compared to that of the spring $E_1$, and the whole body behaves as the springs $E_0$ and $E_1$ in series. For relatively high frequencies, $(\omega\tau)^2 \gg 1$, the resistance of the dashpot is very high, so that the Kelvin-Voigt body becomes stiff and the whole SLS body behaves as the spring $E_0$ alone. Thus, more model bodies must usually be combined in order to describe the response in a wider interval of frequencies.
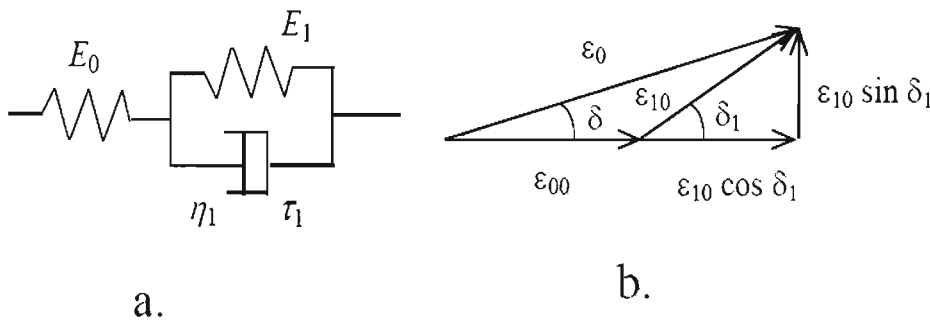


Figure 13. Standard linear solid: $\delta_1$ – shift between stress and strain in the Kelvin-Voigt body. $\delta$ – the resultant shift.

*General Standard Linear Solid (GSLS)*

This body is obtained by adding more Kelvin-Voigt bodies to the standard linear solid (Figure 14a). The resultant phase angle and complex modulus are (Menčík et al., 2004):

$$\tan \delta = \left( \sum_i \frac{1}{E_i} \frac{\omega \tau_i}{1+(\omega \tau_i)^2} \right) \Big/ \left( \frac{1}{E_0} + \sum_i \frac{1}{E_i} \frac{1}{1+(\omega \tau_i)^2} \right) , \tag{75a}$$

$$\frac{1}{E^*} = \sqrt{\left( \frac{1}{E_0} + \sum_i \frac{1}{E_i} \frac{1}{1+(\omega \tau_i)^2} \right)^2 + \left( \sum_i \frac{1}{E_i} \frac{\omega \tau_i}{1+(\omega \tau_i)^2} \right)^2} , \tag{75b}$$

where $E_0$ is the elastic modulus of the „lonely" spring; the index $i$ in the sums varies from 1 to the number $n$ of Kelvin-Voigt bodies. (The moduli can be replaced by compliances $C_i = 1/E_i$.)

This model is suitable if the system is excited by harmonic force and the displacement is measured. If the system is excited by harmonic displacement and the force is measured as the response, the Maxwell variant of general standard linear solid (Figure 14b) can be more appropriate. For this case,

$$\tan \delta = \left( \sum_i E_i \frac{\omega \tau_i}{1+(\omega \tau_i)^2} \right) \Big/ \left( E_0 + \sum_i E_i \frac{1}{1+(\omega \tau_i)^2} \right) , \tag{76a}$$

$$E^* = \sqrt{\left( E_0 + \sum_i E_i \frac{(\omega \tau_i)^2}{1+(\omega \tau_i)^2} \right)^2 + \left( \sum_i E_i \frac{\omega \tau_i}{1+(\omega \tau_i)^2} \right)^2} . \tag{76b}$$

For $n = 1$, the model is reduced to the Maxwell variant of single standard linear solid.
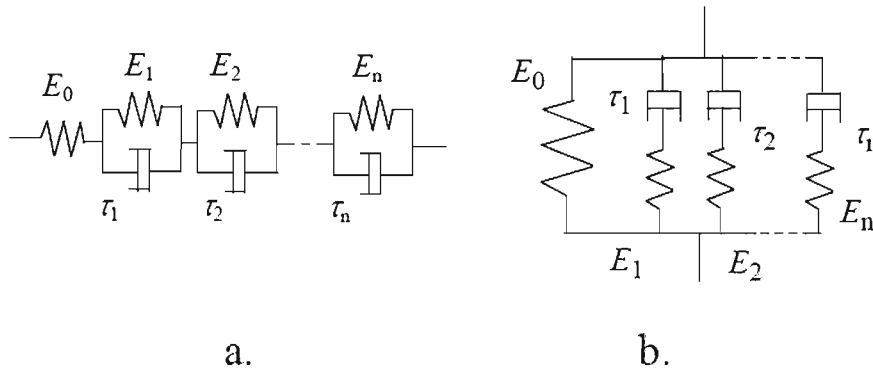


Figure 14. General standard linear solid. a – Kelvin-Voigt variant. b – Maxwell variant.

It is important to note that both variants of (general) standard linear solid are equivalent and can describe the same response (Gross, 1953). If the constants for one variant (e.g. Kelvin-Voigt) are known, it is possible to obtain the values of constants in the conjugated

(here Maxwell) variant of GSLS (with the same number of elements), just by fitting the $E^*(\omega)$ and $\tan \delta(\omega)$ curves by the expressions for this body (Menčík et al., 2004).

## 10.2. Determination of Model Parameters

The values of parameters in the chosen spring-and-dashpot model must be found by experiment. Some indentation devices superimpose a little harmonic signal on the basic load (CSM or DMA mode) and give, as the output, the complex dynamic modulus and phase angle. The measurements are done for several frequencies, and the $E^*(\omega)$ and $\tan\delta(\omega)$ values are fitted by the above expressions for this body. The least squares method can be used, with a suitable nonlinear curve-fitting program. Both curves, $E^*(\omega)$ and $\tan \delta(\omega)$, must be fitted. If only one function (e.g. $\tan\delta$) were fitted, the fit could be very good, but the obtained constants sometimes do not fit the other function ($E^*$) well. It can be recommended to fit $\tan\delta$ first, then $E^*$, then again $\tan \delta$, etc. Often $2 - 6$ steps are sufficient.

The number of Kelvin-Voigt bodies in the model should be chosen with respect to the course of $\tan\delta(\omega)$ in the investigated frequency range; it can loosely correspond to the number of steps or peaks in the curve $\tan\delta(\omega)$ in this interval. (One should be aware of limited range of frequencies available at nanoindentation devices.) For relatively low frequencies ($\omega^2 \tau_i^2 \ll 1$), the K-V body may be replaced by the spring $E_i$ alone (approximately for $\omega < 0.1/\tau_i$). For relatively high frequencies, the body may be removed from the model. This is possible for all K-V bodies with $\tau_i > 10/\omega$. Generally, the viscoelastic properties of a certain K-V body play a role in the range about $0.1 < \omega\tau_i < 10$. As the stiffness of a K-V body changes continuously, it is possible to choose fix retardation times $\tau_i$, scaled in decades; for example $\tau_1 = 1$ s, $\tau_2 = 10$ s, $\tau_3 = 100$ s, etc. Solver then must seek only the constants $E_0, E_1$, etc.

Several general notes must also be made here regarding the indentation measurement of hardness and elastic modulus under harmonic load. If they should be credible, they must be accompanied with the information about all conditions of measurement, including the duration of load increase and the dwell before unloading, as they all influence the results.

Hardness, defined as the mean contact pressure (14), is calculated from the contact area obtained via contact depth $h_c$. According to Eq. (9), the contact depth depends on the total depth (which depends on the duration of loading), and thus also on the contact stiffness. One must keep in mind that two contact stiffnesses can be obtained in the tests: the unloading contact stiffness $S$, calculated according to Eq. (5), and harmonic contact stiffness $S_f$, characterizing the response to harmonic load and calculated according to Eq. (7). The contact depth $h_c$ must always be calculated using the unloading contact stiffness. The additional harmonic oscillations in the CSM (DMA) mode are very small and virtually do not influence the $F$-$h$ curve (Oliver and Pharr, 1992). Hardness (14) is thus independent of the excitation frequency (Menčík et al., 2005), though this fact may look strange. As a simple alternative measure of apparent stiffening of viscoelastic materials at higher frequencies, the index of sensitivity to harmonic load may be used, defined by Menčík et al. (2005) as the ratio of the harmonic and unloading contact stiffness for the same contact depth:

$$q_f = S_f / S . \tag{77}$$

This index can be used to evaluate the influence of frequency or other factors, or to compare various materials.

Elastic modulus under harmonic load depends on the excitation frequency,

$$E_{r,f}{}^* = \frac{\sqrt{\pi}}{2\beta} \frac{S_f}{\sqrt{A}} \quad .$$

(78)

The contact area $A$ must again be calculated using the monotonic unloading contact stiffness, while $S_f$ in the numerator is the harmonic contact stiffness $F_0/h_0$ for the same contact depth. Some nanoindentation devices give the in-phase component of the expression $F_0/h_0$ („extracted" from the measured $F_0$ and $h_0$ values in the device with respect to its inner compliance and damping). In such case, the modulus, calculated according to Eq. (78), corresponds to the storage modulus $E'$. One must therefore be sure what quantities he or she will work with. More about testing under harmonic load can be found, for example, in Herbert et al. (2008), Menčík et al. (2005), Huang et al. (2005), or Odegard et al. (2005).

## 11. Creep and Viscosity

The term creep denotes very slow irreversible deforming under constant load. It appears in metals, glasses or ceramics at high temperatures, but also in polymers, soft metals and some other materials at common temperatures; examples are bitumen or lead. In principle, all solids can be regarded as visco-elastic-plastic, with the individual components of deformation depending on the material, loading conditions and environment. This holds also for the initial stage of creep. Fortunately, in the steady-state stage of creep the delayed elastic processes have ceased and the deforming continues only due to viscous flow, so that the response can be characterized by viscosity. The dynamic viscosity $\eta$ is the proportionality constant between shear stress $\tau$ and shear strain rate:

$$\dot{\gamma} = d\gamma/dt = \tau/\eta \quad .$$

(79)

This Newton's law for viscous liquids is analogous to Hooke's law for elastic solids, $\gamma = \tau/G$, with $t$ corresponding to $\gamma$, and $\eta$ corresponding to shear modulus $G$. This visco-elastic analogy enables direct use of known solutions for elastic problems to the analysis of slow viscous deforming, just by replacing the strains by strain rates, or the characteristic deformation $y$ of an elastic body by the velocity $\dot{y}$ of deforming a similar viscous body, and replacing the shear modulus by dynamic viscosity. If a body is deformed only by viscous flow, and if the stress is constant, also the velocity of deforming is constant and the total deformation (or increase in deformation) during time $t$ is simply $y = \dot{y}_j t$; otherwise it is obtained as:

$$y = \int \dot{y}(t) \, dt \quad ,$$

(80)

where the instantaneous velocity $\chi(t)$ depends on the instantaneous stress $\sigma(t)$. Formulae with elastic solutions for many simple bodies and load cases can be found, e.g., in Roark (1989).

Dynamic viscosity $\eta$ can be measured by various methods, including indentation. The simplest approach uses constant load and measures indenter displacement $h(t)$ as a function of time. Again, formula (47) can be used. For practical reasons, Maxwell body (spring and dashpot in series, Figure 9b) is most suitable, with the creep compliance function

$$J(t) = C_0 + c_v\, t \,. \tag{81}$$

$C_0$ characterizes all deformations that do not depend on time, i.e. the instantaneous and delayed elastic deformations, plastic deformations, and also viscous deformations that have occurred before the beginning of creep measurement.

The viscous compliance $c_v$ in indentation tests is related to the dynamic viscosity $\eta$ by Eq. (57). Combination of Eqs. (49), (81) and (57) gives

$$h^m(t) \;=\; K\,F\left(C_0 + \frac{1-\nu}{2\eta}t\right) \;=\; k_0 + k_1 t \,, \tag{82}$$

where $k_0$ and $k_1$ are regression constants, and $m$ and $K$ are constants for indenter geometry, defined at the beginning of Section 9; for a pointed indenter, $m = 1.5$ and $K = \pi/(2\tan\alpha)$. After fitting the $h^m(t)$ data by linear regression function (82), the dynamic viscosity is obtained as

$$\eta = K\,F\,(1-\nu)\,/\,(2k_1)\,; \tag{83}$$

if incompressibility ($\nu = 0.5$) is assumed, $\eta = KF/(4k_1)$. From papers about viscosity measurement by indentation, Cseh et al. (1997) and Sakai and Shimizu (2001) can be recommended.

## CONCLUSION

Today, nanoindentation (instrumented indentation) enables the determination of many important material characteristics, such as elastic modulus and hardness, yield strength and stress-strain curves for elastic-plastic materials, but also parameters in rheological models for viscoelastic response. Indentation devices and methods have been developed permanently, and more and more sophisticated procedures for analysis appear, often in combination with the finite element modeling and other tools. Nevertheless, very often simple models and methods are quite sufficient (also because they are sometimes based on a very elaborate analysis). However, one must be avare of the limited validity of a particular model. This chapter has brought an overview of various simple models, with the explanation how they were derived and what are their limits. In this way it can help in the choice of a suitable model and formulae and test conditions. The text was accompanied by numerous references, which can facilitate further study.

## ACKNOWLEDGMENTS

## REFERENCES

Baker, S. P., Cook, R. F., Corcoran, S. G., and Moody, N. R., editors. (2001). *Fundamentals of Nanoindentation and Nanotribology II. Mat. Res. Soc. Symp. Proc., Vol. 649*, MRS, Warrendale, Pennsylvania.

Barenblatt, G. I. (1996). *Scaling, Self-similarity, and Intermediate Asymptotics*. Cambridge: Cambridge University Press.

Basu, S., Moseson, A., and Barsoum, M. W. (2006). On the determination of spherical nanoindentation stress-strain curves. *J. Mater. Res., Vol. 21, No. 10*, 2628 – 2637.

Bec, S., Tonck, A., Georges, J. M., Georges, E., and Loubet, J. L. (1996). Improvements in the indentation method with a surface force apparatus. *Phil. Mag. A, Vol. 74*, 1061 – 1072.

Bec, S., Tonck, A., and Loubet, J. L. (2006). A simple guide to determine elastic properties of films on substrates from nanoindentation experiments. *Philosophical Magazine, Vol. 86, No. 33-35*, 5347 – 5358.

Bhattacharya, A.K., and Nix, W. D. (1988). Analysis of elastic and plastic deformation associated with indentation testing of thin films on substrates. *Int. J. Solids Struct., Vol. 24, No. 12*, 1287 - 1298.

Burnett, P. J., and Rickerby, D. S. (1987). The mechanical properties of wear resistant coatings I, II: Modelling of hardness behaviour. *Thin Solid Films, Vol. 148*, 41 - 65.

Cao, Y. P., and and Lu, J. (2004). A new method to extract the plastic properties of metal materials from an instrumented spherical indentation loading curve. *Acta Materialia, Vol. 52*, 4023 – 5032.

Chen, J., and Bull, S. J. (2009). Relation between the ratio of elastic work to the total work of indentation and the ratio of hardness to Young´s modulus for a perfect conical tip. *J. Mater. Res., Vol. 24, No. 3*, 590 – 598.

Cheng, L., Scriven, L.E., and Gerberich, W.W. (1998). Viscoelastic analysis of micro- and nanoindentation. pp. 193 - 198 in: Moody et al. (1998).

Cheng, L., Xia, X., Yu, W., Scriven, L. E., and Gerberich, W. W. (2000). Flat-punch indentation of a viscoelastic material. *J. Polymer Sci. B: Polymer Phys. Vol. 38, No. 1*, 10 – 22.

Cheng, L., Xia, X., Scriven, L. E., and Gerberich, W. W, (2005). Spherical-tip indentation of viscoelastic material. *Mechanics of Materials, Vol. 37, No. 1*, 213 – 226.

Cheng, Y. T., and Cheng, C. M. (1999). Scaling relationships in conical indentation of elastic-perfectly plastic solids. *Int. J. Solids Structures, Vol. 36*, 1231 – 1243.

Cheng, Y. T., and Cheng, C. M. (2004). Scaling, dimensional analysis, and indentation measurements. *Mat. Sci. Eng. R 44*, 91 - 149.

Cheng, Y. T., and Cheng, C. M. (2005a). Relationships between initial unloading slope, contact depth, and mechanical properties for conical indentation in linear viscoelastic solids. *J. Mater. Res., Vol. 20, No. 4*, 1046 – 1053.

Cheng, Y. T., and Cheng, C. M. (2005b). Relationships between initial unloading slope, contact depth, and mechanical properties for indentation in linear viscoelastic solids using axisymmetric indenters of arbitrary profiles. *Appl. Phys. Lett., Vol. 87*, Art. No. 111914.

Chudoba, T., and Richter, F. (2001). Investigation of creep behaviour under load during indentation experiments and its influence on hardness and modulus results. *Surf. Coat. Technol., Vol. 148*, 191 – 198.

Cseh, G., Chinh, N.Q., Tasnádi, A., and Juhász, A. (1997). Indentation test for the investigation of high-temperature plasticity of materials. *J. Mater. Sci., Vol. 32*, 5107 – 5111.

Doerner, M.F., and Nix, W.D. (1986). A method for interpreting the data from depth-sensing indentation instruments. *J. Mater. Res., Vol. 1, No. 4*, 601 – 609.

Feng, G., and Ngan, A. H. V. (2002). Effects of creep and thermal drift on modulus measurement using depth-sensing indentation. *J. Mater. Res., Vol. 17, No. 3*, 660 – 668.

Field, J., and Swain, M.V. (1993). A simple predictive model for spherical indentation. *J. Mater. Res., Vol. 8, No. 2*, 297 – 306.

Findley, W. N., Lai, J. S., and Onaran. K. (1976). *Creep and relaxation of nonlinear viscoelastic materials*. New York: Dover Publications, Inc.

Fischer-Cripps, A.C. (2002, 2nd Ed. 2004). *Nanoindentation*. New York, Springer.

Fujisawa, N., and Swain, M.V. (2006). Effect of unloading strain rate on the elastic modulus of a viscoelastic solid determined by nanoindentation. *J. Mater. Res., Vol. 21, No. 3*, 708 – 714.

Gao, H., Chiu, C.H., and Lee, J. (1992). Elastic contact versus indentation modelling of multilayered materials. *Int. J. Solids Structures, Vol. 29*, 2471 – 2492.

Gao, X. L. (2006). New expanding cavity model for indentation hardness including strain-hardening and indentation size effects. *J. Mater. Res., Vol. 21, No. 5*, 1317 – 1326.

Giannakopoulos, A. E. (2006). Elastic and viscoelastic indentation of flat surfaces by pyramid indentors. *J. Mech. Phys. Solids, Vol. 54*, 1305-1332.

Goble, D. L., and Wolff, E. G. (1993). Strain-rate sensitivity index of thermoplastics. *J. Mater. Sci., Vol. 28*, 5986 – 5994.

Gross, B. (1953). *Mathematical structure of the theories of viscoelasticity*. Paris: Hermann.

Haddad, Y.M. (1995). *Viscoelasticity of Engineering Materials*, London, Chapman and Hall.

Herbert, E. G., Pharr, G. M., Oliver, W. C., Lucas, B. N., and Hay, J. L. (2001). On the measurement of stress-strain curves by spherical indentation. *Thin Solid Films, Vol. 398 – 399*, 331 – 335.

Herbert, E. G., Oliver, W. C., and Pharr, G. M. (2006). On the measurement of yield strength by spherical indentation. *Phil. Mag., Vol. 86, Nos. 33-35*, 5521 – 5539.

Herbert, E. G., Oliver, W. C., and Pharr, G. M. (2008). Nanoindentation and the dynamic characterization of viscoelastic solids. *J. Phys. D: Appl. Phys. Vol. 41*, 1 – 9.

Hochstetter, G., Jimenez, A., Cano, J. P., and Felder, F. (2003). An attempt to determine the true stress-strain curves of amorphous polymers by nanoindentation. *Tribol. Int., Vol. 36, No. 12,* 973 – 985.

Huang, G., Wang, B., and Lu, H. (2004). Measurements of viscoelastic functions of polymers in the frequency-domain using nanoindentation. *Mech. Time-dependent. Mater., Vol. 8, No. 4,* 345 – 364.

Huber, N., and Tyulyukovskiy, E. (2004). A new loading history for identification of viscoplastic properties by spherical indentation. *J. Mater. Res., Vol. 19, No. 1,* 101 – 113.

Huber, N., Tyulyukovskiy, E., and Kraft, O. (2006). On the analysis of the stress-strain behaviour of thin metals on substrates using nanoindentation. *Philosophical Magazine, Vol. 86, No. 33-35,* 5505 – 5519.

ISO 14577 (2002 – 2007). *Metallic materials – Instrumented indentation test for hardness and materials parameters. Part 1: Test method. Part 4: Test methods for metallic and non-metallic coatings.* International Organization for Standardization (ISO).

Johnson, K. L. (1970). The correlation of indentation experiments. *J. Mech. Phys. Solids, Vol. 18,* 115 – 126.

Johnson, K.L. (1985). *Contact mechanics,* Cambridge, Cambridge University Press.

Jönsson, B., and Hogmark, S. (1984). Hardness measurement of thin films. *Thin Solid Films, Vol. 114,* 257 – 269.

Korsunsky, A. M., McGurk, M. R., Bull, S. J., and Page, T. F. (1998). On the hardness of coated systems. *Surf. Coat. Technol., Vol. 99, No. 1-2,* 171 – 183.

Kucharski, S., and Mróz, Z. (2001). Identification of elasto-plastic hardening parameters of metals from spherical indentation tests. *Mat. Sci. Engng, Vol. 318, Nos. 1-2,* 65 – 76.

Lee, S., and Knauss, W. G. (2000). A note on the determination of relaxation and creep data from ramp tests. *Mech. Time-dependent Mater., Vol. 4, No. 1,* 1 – 7.

Lee, E.H., and Radok, J. R. M. (1960). The contact problem for viscoelastic bodies. *Trans. ASME, Series E, Journal of Applied Mechanics, Vol. 27,* 438 – 444.

Lu, H., Wang, B., Ma, J., Huang, G., and Viswanathan, H. (2003). Measurement of creep compliance of solid polymers by nanoindentation. *Mech. Time-dependent Mater., Vol. 7, No. 3-4,* 189 – 207.

Lucas, B. N., Oliver, W. C., Pharr, G. M., and Loubet, J. L. (1997). Understanding time dependent deformation during indentation testing. pp. 233 – 238 in: W. W. Gerberich, H. Gao. J. E. Sundgren, and S. P. Baker (editors): *Thin Films: Stresses and Mechanical Properties VI, Mater. Res. Soc. Symp. Proc. 436.* Warrendale, PA: Mat. Res. Soc.

Ma, D., Ong, C. W., Lu, J., and He, J. (2003). Methodology for the evaluation of yield strength and hardening behavior of metallic materials by indentation with spherical tip. *J. Appl. Phys., Vol. 94, No. 1.* 288 – 294.

Malzbender, J. (2005). Comment on the determination of mechanical properties from the energy dissipated during indentation. *J. Mater. Res., Vol. 20, No. 5,* 1090 – 1092.

Malzbender, J., and de With, B. (2000). The use of the loading curve to assess soft coatings. *Surf. Coat. Technol., Vol. 127,* 266 – 273.

Menčik, J. (1996). *Mechanics of Components with Treated or Coated Surfaces.* Dordrecht: Kluwer Academic Publishers.

Menčik, J. (2006). Determination of stress-strain curves by instrumented indentation. *23rd Danubia Adria Symposium on Experimental Methods in Solid Mechanics, Podbanské, 26 – 29 Sept 2006,* pp. 31 – 32. Žilina: University of Žilina, Slovakia. ISBN 80-8070-589-5.

Menčik, J., and Swain, M.V. (1994). Characterisation of materials using micro-indentation tests with pointed indenters. *Materials Forum, Vol. 18*, 277 – 288.

Menčik, J., Munz, D., Quandt, E., Weppelmann, E.R., and Swain, M.V. (1997). Determination of elastic modulus of thin layers using nanoindentation. *J. Mater. Res., Vol. 12, No. 9*, 2475 – 2484.

Menčik, J., Rauchs, G., Belouettar, S., Bardon, J., and Riche, A. (2004). Modeling of response of viscoelastic materials to harmonic loading. *Int. Conf. Engineering Mechanics 2004. Svratka, May 10-13, 2004*, Prague: Institute of Thermomechanics ASCR, ISBN 80-85918-88-9, pp. 187 – 188, full paper on CD-ROM.

Menčik, J., Rauchs, G., Bardon, and J., Riche, A. (2005). Determination of elastic modulus and hardness of viscoelastic-plastic materials by instrumented indentation under harmonic load. *J. Mater. Res., Vol. 20, No. 10*, 2660 – 2669.

Menčik, J., He, L.H., and Swain, M. V. (2009). Determination of viscoelastic-plastic material parameters of biomaterials by instrumented indentation. *J. Mech. Behav. Biomed., 2*, 318 – 325.

Mesarovic, S. Dj., and Fleck, N. A. (1999). Spherical indentation into elastic-plastic solids. *Proc. R. Soc. Lond. A, Vol. 455*, 2707 – 2728.

Moody, N.R., Gerberich, W.W., Burnham, N., and Baker, S. P., editors. (1998). *Fundamentals of Nanoindentation and Nanotribology. Mat. Res. Soc. Symp. Proc., Vol. 522*. Warrendale, Pennsylvania: MRS.

Němeček, J. (2009). Creep effects in nanoindentation of hydrated phases of cement pastes. *Materials Characterization, Vol. 60*, 1028 – 1034.

Ngan, A. H. W., and Tang, B. (2002). Viscoelastic effects during unloading in depth-sensing indentation. *J. Mater. Res., Vol. 17, No. 10*, 2604 – 2610.

Ni, W., Cheng, Y-T., Cheng, Ch-M., and Grummon, D. S. (2004). An energy-based method for analyzing instrumented spherical indentation experiments. *J.Mater. Res., Vol. 19, No. 1*, 149 – 157.

Odegard, G. M., Gates, T. S., and Herring, H. M. (2005). Characterization of viscoelastic properties of polymeric materials through nanoindentation. *Exper. Mech., Vol. 45, No. 2*, 130 – 136.

Ogasawara, N., Chiba, N., and Chen, X. (2005). Representative strain of indentation analysis. *J. Mater. Res., Vol. 20, No. 8*, 2225 – 2234.

Oliver, W. C. (2001). Alternative technique for analzying instrumented indentation data. *J. Mater. Res., Vol. 16*, 3202 – 3206.

Oliver, W.C., and Pharr, G. M. (1992). An improved technique for determining hardness and elastic modulus using load and displacement sensing indentation experiments. *J. Mater. Res., Vol. 7, No. 6*, 1564 – 1583.

Oliver, W. C., and Pharr, G. M. (2004). Measurement of hardness and elastic modulus by instrumented indentation: Advances in understanding and refinements to methodology. *J. Mater. Res., Vol. 19, No. 1*, 3 – 20.

Oyen, M. L. (2005). Spherical Indentation Creep Following Ramp Loading. *J. Mater. Res., Vol. 20, No. 8*, 2094 – 2100.

Oyen, M. L. (2006). Analytical Techniques for Indentation of Viscoelastic Materials. *Philosophical Magazine, Vol. 86, No. 33-35*, 5625 – 5641.

Oyen, M. L., and Cook, R. F. (2003). Load-displacement behavior during sharp inentation of viscous-elastic-plastic materials, *J. Mater. Res., Vol. 18, No. 1*, 139 – 150.

Page, T., and Bull, S. J. (2006). Measuring and modelling the instrumented indentation (nanoindentation) response of coated systems. *Philosophical Magazine, Vol. 86, No. 33-35*, 5331 – 5346.

Pharr, G. M., and Bolshakov, J. (2002). Understanding nanoindentation unloading curves. *J. Mater. Res., Vol. 17, No. 10*, 2660 – 2671.

Pharr, G. M., Strader, J. H., and Oliver, W. C. (2009). Critical issues in making small-depth mechanical property measurements by nanoindentation with continuous stiffness measurement. *J. Mater. Res., Vol. 24, No. 3*, 653 – 666.

Radok, J. R. M. (1957). Viscoelastic stress analysis. *Q. App. Mat., Vol. 15*, 198 – 202.

Rar, A., Song. H., and Pharr, G. M. (2001). Assessment of New Relation for the Elastic Compliance of a Film-Substrate System. paper L10.10 in: C. S. Ozkan, L. B. Freund, R. C. Cammarata, H. Gao (editors): *Thin Films: Stresses and Mechanical Properties IX, Mat. Res. Soc. Symp. Proc., Vol. 695*. Warrendale, Pennsylvania: MRS.

Roark, R.J. (1989). *Roark's formulas for stress and strain. International Edition*. New York: McGraw-Hill.

Saha, R., and Nix, W. D. (2002). Effects of the substrate on the determination of thin film mechanical properties by nanoindentation. *Acta Materialia, Vol. 50*, 23 – 38.

Sakai, M. (1993). Energy principle of the indentation-induced inelastic surface deformation and hardness of brittle materials. *Acta metall.mater., Vol. 41, No. 6*, 1751 – 1758.

Sakai, M. (1999). The Meyer hardness: A measure for plasticity? *J. Mater. Res., Vol. 14, No. 9*, 3630 – 3639.

Sakai, M. (2009). Substrate-affected indentation contact parameters of elastoplastic coating/substrate composites. *J. Mater. Res., Vol. 24, No. 3*, 831 – 843.

Sakai, M., and Shimizu, S. (2001). Indentation rheometry for glass-forming materials. *J. Non-crystalline Solids, Vol. 282, No. 2-3*, 236 – 247.

Shimizu, S., Yanagimoto, T., and Sakai, M. (1999). The pyramidal indentation load-depth curve of viscoelastic materials. *J. Mater. Res., Vol. 14, No. 10*, 4075 – 4086.

Sneddon, I. N. (1965). The relation between load and penetration in the axisymmetric Boussinesq problem for a punch of arbitrary profile. *Int. J. Engng. Sci., Vol. 3*, 47 – 51.

Strojny, A., and Gerberich, W. W. (1998). Experimental analysis of viscoelastic behavior in nanoindentation. pp. 159 – 164 in: Moody et al. (1998).

Szirtes, T. (1997). *Applied Dimensional Analysis and Modeling*. New York: McGraw-Hill.

Tabor. H. (1951). *Hardness of Metals*. Oxford: Clarendon Press.

Tan, M. (2006). A study of indentation work in homogeneous materials. *J. Mater. Res., Vol. 21, No. 6*, 1363 – 1374.

Tschoegl, N.W. (1989). *The Phenomenological Theory of Linear Viscoelastic Behavior*. Berlin: Springer-Verlag.

Tyulyukovskiy, E., and Huber, N. (2006). Identification of viscoplastic material parameters from spherical indentation. *J. Mater. Res., Vol. 21, No. 3*, 664 – 676 (Part I). 677 – 684 (Part II).

Wahl, K. J., Huber, N., Mann, A. B., Bahr, D. F., and Cheng, Y-T., editors. (2005). *Fundamentals of Nanoindentation and Nanotribology III. Mat. Res. Soc. Symp. Proc., Vol. 841*. Warrendale, Pennsylvania: MRS.

Wang, L., and Rokhlin, S. I. (2006). On determination of material parameters from loading and unloading responses in nanoindentation with a single sharp indenter. *J. Mater. Res., Vol. 21, No. 4*, 995 – 1011.

Wei, P. J., and Lin, J. F. (2009). Modified method for continuous stiffness measurement. *J. Mater. Res.*, *Vol. 24, No. 3*, 599 – 606.

Yu, W., and Blanchard, J. P. (1996). An elastic-plastic indentation model and its solutions. *J. Mater. Res.*, *Vol. 11, No. 9*, 2358 – 2367.

Zhang, C.Y., Zhang, Y. W., and Zeng, K. Y. (2004). Extracting the mechanical properties of a viscoelastic polymeric film on a hard elastic substrate. *J. Mater. Res.*, *Vol. 19, No. 10*, 3053 – 3061.

Zhang, C.Y., Zhang, Y. W., Zeng, K. Y., and Shen, L. (2005). Nanoindentation of polymers with a sharp indenter. *J. Mater. Res.*, *Vol. 20, No. 6*, 1597 – 1605.